Journal of the Mechanics and Physics of Solids ▮ (▮▮▮▮) ▮▮▮–▮▮▮

Contents lists available at SciVerse ScienceDirect

Journal of the Mechanics and Physics of Solids

journal homepage: www.elsevier.com/locate/jmps

Phenomenological crystal plasticity modeling and detailed micromechanical investigations of pure magnesium

Jing Zhang, Shailendra P. Joshi *

Department of Mechanical Engineering, National University of Singapore, Singapore 117576, Singapore

ARTICLE INFO

Article history:
Received 15 March 2011
Received in revised form
14 October 2011
Accepted 4 January 2012

Keywords:
Pure magnesium
Single crystal plasticity
Constitutive laws
Slip and twinning
Micromechanics

ABSTRACT

We present a single crystal plasticity model for pure Mg incorporating slip and deformation twinning. The model uses the basic framework of Kalidindi (1998), but proposes constitutive descriptions for the slip and twin evolution and their interactions that are motivated by experimental observations. Based on compelling experimental evidences, we distinguish between the constitutive descriptions of the tension and compression twinning to better represent their roles in the overall hardening of Mg single crystals. With these improved phenomenological descriptions, we first calibrate material parameters for the different slip and twin modes by performing three-dimensional simulations mimicking the plane-strain compression experiments by Kelley and Hosford (1967, 1968) on single crystal pure Mg. In doing so, these computational responses are critically compared with their corresponding orientation-dependent microscopic (slip and twin activities) and macroscopic (stress–strain responses) experimental observations. Then, the calibrated parameters are used to predict several other experimental results on pure single- and poly-crystal Mg under different loading conditions. We also investigate the role of pre-existing heterogeneities such as initial twin population and stiff, elastic inclusions on the single crystal macroscopic and microscopic responses. Microstructural characteristics show that such heterogeneities strongly influence the local and global evolution of the slip and twin activities, and in some cases modulate the strength anisotropy that is commonly observed in monolithic single crystals. These results may provide useful indicators toward designing novel composite Mg microstructures.

1. Introduction

Magnesium (Mg) and its composites are potential candidates for structural applications ranging from energy-savvy automotive and aerospace sectors to biomedical components, due to its low mass density (~35% lighter than aluminum) and excellent biocompatibility. There has been a renewed emphasis toward developing novel micro-architectures with impressive specific strengths (strength/density) using pure Mg or its alloys by inducing barriers to plastic deformation through a variety of techniques including grain size refinement, nano-reinforcements, or combinations thereof (Gharghouri et al., 1998; Xu et al., 2007; Zhong et al., 2007).[1] For example, starting with pure Mg matrix, Zhong et al.

* Corresponding author. Tel.: +65 6516 4496; fax: +65 6779 1459.
E-mail address: Shailendra@nus.edu.sg (S.P. Joshi).

[1] Although Mg alloys may be popular starting materials from a practical standpoint, pure Mg is a good model material for fundamental investigations for such novel attempts.

0022-5096/$ - see front matter © 2012 Elsevier Ltd. All rights reserved.
doi:10.1016/j.jmps.2012.01.005

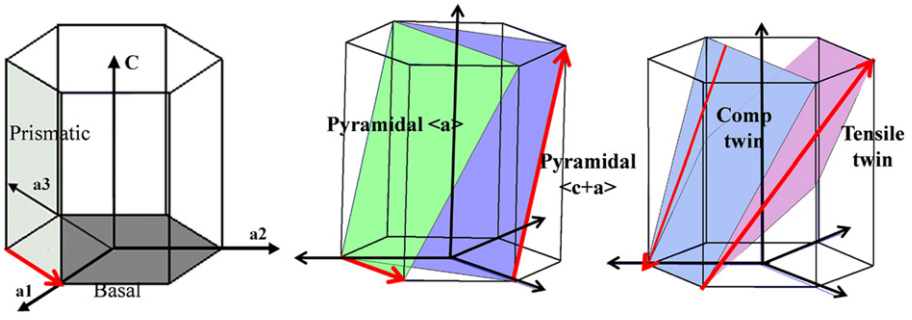

Fig. 1. Schematic diagrams of slip and twin systems in magnesium.

(2007) and Habibi et al. (2010) have recently shown that its mechanical performance including the yield strength, hardening and ductility of pure Mg can be dramatically improved by adding dilute amounts of nano-scaled reinforcements. These significant improvements are intimately tied to the manner in which the underlying deformation mechanisms are modulated by the small-scaled heterogeneities and in order to optimally design such microstructures it is important to develop prognostic tools that enable their detailed understanding. A cleaner understanding of the inelastic deformation mechanisms in Mg is also vital to successful applications. However, modeling such intricate holistic responses is a challenging task because of the myriad interactions between the different deformation mechanisms (Fig. 1) that prevail in this hexagonal close-packed (HCP) crystal structure (Christian and Mahajan, 1995). In Mg, the basal slip (i.e. $(0001)\langle 11\bar{2}0\rangle$)[2] and two non-basal slip modes—the prismatic $\{10\bar{1}0\}\langle 11\bar{2}0\rangle$ and the pyramidal $\langle a\rangle(\{10\bar{1}1\}\langle 11\bar{2}0\rangle)$ provide deformation parallel to the basal plane only. Thus, even when these slip systems are activated simultaneously they cannot accommodate arbitrary plastic deformation. Furthermore, the secondary pyramidal $\langle c+a\rangle$ slip, $(\{11\bar{2}2\}\langle 11\bar{2}3\rangle)$ which provides another non-basal (out-of-basal-plane Burgers vector) deformation is relatively difficult to activate at room temperature due to its high critical resolved shear stress (CRSS). Therefore in Mg, like in most HCP metals, deformation twinning (DT) provides an additional mechanism to accommodate *c*-axis deformation, which is intimately tied to the lattice parameter, *c*/*a* ratio (Yoo, 1981). In Mg, the most commonly observed DT mode is the $\{10\bar{1}2\}\langle 10\bar{1}1\rangle$ extension (tensile) twinning when the *c*-axis experiences tension, whereas the less common, $\{10\bar{1}1\}$ and $\{30\bar{3}4\}$ contraction (compressive) twinning modes may sometimes occur under *c*-axis compression (Reed-Hill and Robertson, 1957a, 1957b; Yoshinaga et al., 1973).[3] $\{10\bar{1}3\}$ tensile twinning, is also reported in experiments as a double twin mode (Ma et al., 2011). The interactions between aforementioned deformation mechanisms result in a significant anisotropy in the macroscopic response for both, single and textured polycrystalline Mg and their composites. Especially, the relative activities of the slip and DT modes are strongly orientation-dependent and influence the hardening behavior (Caceres and Lukac, 2008), texture evolution (Agnew et al., 2001; Brown et al., 2005), crack propagation (Ando et al., 2006) and ductility (Miura et al., 2005). Kelley and Hosford (1968, 1967) (also referred to as K–H in this paper) and Wonsiewicz (1966) performed comprehensive investigations on pure Mg single crystals at both room and higher temperatures. Their plane-strain compression experiments have led to a detailed account of the orientation-dependent macroscopic and microscopic response of pure Mg single- and poly-crystals. Recently, Chapuis and Driver (2010) also performed experiments on single crystal pure Mg for a limited types of orientations, but also explored the temperature effects.

A variety of modeling approaches have been developed at the continuum scale to describe the rich mechanics for a broad class of HCP metals including Mg (Brown et al., 2005; Graff et al., 2007; Kalidindi, 1998; Proust et al., 2007; Roters et al., 2010; Salem et al., 2005; Staroselsky and Anand, 2003; Tomé et al., 1991; Wang et al., 2010). Among them, sophisticated self-consistent polycrystal plasticity models (e.g. Brown et al., 2005; Tomé et al., 1991; Wang et al., 2010) incorporating dislocation slip and DT have been developed to study the macroscopic behaviors including strain hardening, texture evolution and internal stress variation. These *top–down* approaches are elegant in that they are well-suited to model polycrystalline behaviors and in the process, obtain estimates of single crystal parameters. On the other hand, it is also useful to develop a *bottom–up* approach relying on single crystal plasticity (SCP) whose constitutive parameters for the individual slip and twin modes are identified by critically comparing them with single crystal experiments at the macroscopic and microscopic levels. Once identified, they may be employed in predicting several features in single as well as polycrystalline Mg such as the orientation-dependent stress–strain responses, hardening behaviors, texture evolution, fracture, and so on. Compared to the homogenized approaches, the bottom–up approach serves as a model length-scale to admit newer features that are discovered in sub-scale experiments and simulations (e.g. molecular/dislocation dynamics) For example, they may prove valuable in distinguishing between the mechanics of Mg at conventional length-scales and the emerging field of the mechanics at small length-scales (Byer et al., 2010; Lilleodden, 2010). It is also naturally

[2] Throughout the paper (*hkil*) indicates a specific slip/twin plane, [*uvwx*] specific slip/twin direction, {*hkil*} indicates family of a particular slip/twin plane and $\langle uvwx\rangle$ indicates family of particular slip/twin directions.

[3] The $\{10\bar{1}1\}\langle 10\bar{1}\bar{2}\rangle$ compression twins have been widely reported. It is believed that the $\{30\bar{3}4\}$ twin is a sequence of $\{10\bar{1}1\}$ twins (Reed-Hill, 1960).

Please cite this article as: Zhang, J., Joshi, S.P., Phenomenological crystal plasticity modeling and detailed micromechanical investigations of pure magnesium. J. Mech. Phys. Solids (2012), doi:10.1016/j.jmps.2012.01.005

amenable in probing the local deformation characteristics in the neighborhood of discrete heterogeneities such as grain boundaries (e.g. Choi et al., 2010) and twin boundaries, inclusions, cracks and so on. Further, they can be well suited to incorporating the roles of such interfaces in modulating twin and slip activities (Beyerlein et al., 2010, 2011b).

However, limited efforts have been made to numerically capture the mechanical characteristics of pure Mg single crystals that should serve as a starting point, as much of the focus has been on the polycrystalline Mg and its alloys. Although there are some recent SCP works in literature focusing on single crystal pure Mg (e.g. Izadbakhsh et al., 2011), many of them limit themselves to comparing macroscopic behaviors (i.e. stress–strain responses) of single- and polycrystals. There are very few works that critically corroborate the orientation-dependent evolution of the slip and twin activities with experiments and address their relative importance through physically based arguments. Much of the current progress in HCP SCP owes its roots to the seminal developments by Kalidindi (Kalidindi, 1998; Salem et al., 2005) and Staroselsky and Anand (1998) who included twinning along with slip within the constitutive description. This approach introduces twinning induced plasticity through a phenomenological evolution law for the twin volume fraction (v.f.), modeling it as a pseudo-slip mechanism. Staroselsky and Anand (2003) also included grain boundary sliding to enable improved predictions of an Mg-alloy. Graff et al. (2007) proposed an SCP model for Mg, but they did not explicitly model the lattice reorientation due to DT. One of the highlights of their work is the predicted evolution of the relative slip and twin activities with strain for different crystal orientations tested in K–H experiments. However, it is surprising to note the quantitative corroboration of their predicted stress–strain responses with the K–H experiments in the absence of the DT induced lattice reorientation, especially for twin-friendly crystal orientations. For example, it is difficult to reconcile from their simulations as to why the stress–strain curves for two tensile twin-friendly orientations (orientations E and F in Kelley and Hosford, 1967, 1968) are quite different at large strains (in accordance with the experiments) while their slip activities are predicted to be very similar (cf. Fig. 6e and f in Graff et al., 2007). Also, their hardening functions for the slip and twin systems calibrated with both single-crystal and polycrystal experimental results of K–H lack physical motivation.

An interesting aspect emerging from single crystal experiments is the apparent contradiction between pyramidal $\langle c+a \rangle$ slip and compression twin (CT) in Mg single crystals subjected to the c-axis compression. While some report dominant occurrence of CT (Kelley and Hosford, 1967; Wonsiewicz, 1966; Yoshinaga and Horiuchi, 1963a), others report only the pyramidal $\langle c+a \rangle$ slip (Byer et al., 2010; Lilleodden, 2010), or prevalence of both (Kitahara et al., 2007; Obara et al., 1973). SCP approaches with appropriate constitutive descriptions should be able to discern between such experimental observations under different loading conditions, because these mechanisms may have important implications on the hardening, ductility and failure. This emphasizes the need for descriptions of the slip and twin mechanisms at the single crystal level that are motivated by physical arguments (Christian and Mahajan, 1995; Yoo, 1981). In this regard, recent progress involving transmission electron microscopy (TEM), electron backscatter diffraction (EBSD), neutron diffraction, 3D X-ray diffraction, and to some extent, molecular dynamics (MD) is valuable in advancing our understanding on the evolution of twinning and the competition between the slip and twinning mechanisms in Mg (Al-Samman et al., 2010; Aydiner et al., 2009; Clausen et al., 2008; Groh et al., 2009; Li and Ma, 2009; Serra and Bacon, 1995; Serra et al., 1999; Wang et al., 2009).

A summary of this somewhat long preamble is that although the basic construct for Mg SCP is available in literature, physically based explanation of the constitutive description for slip and twin evolution seems lacking. In some cases the motivation behind the choice of a particular form of the constitutive law is not well-explained. Further, not all models incorporate both tensile and compression twinning (TT and CT) along with the lattice reorientation effects and those that consider them, do not distinguish clearly between their evolution characteristics. In this paper, we present an SCP model for single crystal pure Mg that fundamentally follows along the lines of Kalidindi (1998), but attempts to address the following objectives:

1. To provide improved phenomenological descriptions of slip and twin (CT and TT) v.f. evolution including the slip–slip, twin–slip and twin–twin interactions while retaining the basic structure of the conventional self- and latent-hardening laws.
2. To rigorously characterize the material parameters corresponding to these improved descriptions by simulating the plane-strain compression experiments of K–H and critically corroborating the orientation-dependent macroscopic and microscopic responses (Kelley and Hosford, 1968, 1967) through single crystal simulations.[4]
3. To probe the effect of the DT-induced lattice reorientation on the strain hardening behavior vis-à-vis the twin v.f. evolution and the effect of initial defect population (e.g. initial twin v.f.) on the macroscopic response for twin-friendly orientations.
4. To use the constitutive parameters of single crystal Mg in predicting the macroscopic response of other single crystal (e.g. uniaxial experiments) and polycrystalline pure Mg with different textures.
5. To apply the SCP model in predicting the orientation-dependent micro–macro characteristics of pure Mg single crystals with embedded inclusions in connection with its applicability to Mg composites.

[4] Some, but not all, orientations in K–H experiments may necessitate 3D finite element simulations although the loading is under plane strain condition, as discussed in the subsequent sections in this paper.

Please cite this article as: Zhang, J., Joshi, S.P., Phenomenological crystal plasticity modeling and detailed micromechanical investigations of pure magnesium. J. Mech. Phys. Solids (2012), doi:10.1016/j.jmps.2012.01.005

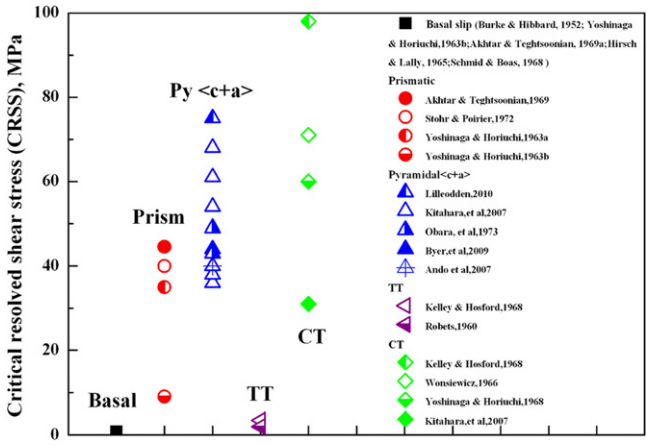

Fig. 2. Experimentally reported room temperature CRSS for slip and twin modes in pure Mg single crystals (Ando et al., 2007; Hirsch and Lally, 1965; Roberts, 1960; Schmid and Boas, 1968; Stohr and Poirier, 1972; Yoshinaga and Horiuchi, 1963b).

With reference to no. 1 above, we note that the classic review by Christian and Mahajan (1995) on deformation twinning provides fundamental insights into the interaction effects between different deformation mechanisms in HCP materials. In this work we do not claim to reconcile all the information provided there. However, an attempt is made to provide arguments for the choice of descriptions wherever possible.

In the next section, we briefly discuss the prevailing experimental observations on single crystal Mg with reference to the deformation mechanisms, their kinetics and the aspects of its constitutive implementation, especially the slip–slip, twin–slip, and twin–twin interactions. In the subsequent sections, these observations are then used to identify the constitutive parameters for the SCP approach and critically compare the simulated results with K–H experiments. Then, we predict the validity of these constitutive parameters for single-crystals and polycrystals under general loading conditions. Finally, we investigate the micro–macro-relationship in pure Mg single crystal matrices with inclusions with reference to Mg composites.

2. Modeling framework

2.1. Deformation mechanisms in pure Mg

In SCP framework, the activity of a slip or twin system is usually governed by a CRSS and a hardening law. Fig. 2 summarizes the CRSS values reported in the literature for the slip and twin modes in pure Mg single crystals at room temperature. In general, basal slip and TT are the easiest to activate as even a small non-zero Schmid factor on these systems can trigger them given that their very low CRSSs, much lower compared to the other modes. There is quite a bit of variation in the CRSS values for the non-basal slip modes and CT. At room temperature, the $\{10\bar{1}0\}$ prismatic and $\{10\bar{1}1\}$ *first-order*[5] pyramidal modes are the next easier slip modes in Mg and have been reported in experiments (Burke and Hibbard, 1952; Couret and Caillard, 1985a, 1985b; Reed-Hill and Robertson, 1958; Yoo and Wei, 1967). Note that in Fig. 2 the experimental CRSS data for pyramidal $\langle a \rangle$ is lacking; however, prismatic and pyramidal $\langle a \rangle$ slips seem to play similar roles (Agnew et al., 2006; Chapuis and Driver, 2010) and in this work we assume identical parameters for these modes. CTs may develop under *c*-axis compression (Kelley and Hosford, 1968; Wonsiewicz, 1966; Yoshinaga and Horiuchi, 1963a) and it is important to account for them because their presence may have implications on the overall ductility (Kitahara et al., 2007; Obara et al., 1973; Byer et al., 2010; Lilleodden, 2010).

The relative slip and twin activities strongly depend on the crystal orientation with respect to the primary loading direction and additional constraints (e.g. as in the case of plane-strain compression). For example, two specimens under plane-strain compression loaded perpendicular to the *c*-axis undergo nearly the same TT process initially, but show remarkably different hardening behaviors after DT-induced lattice reorientation when constrained in either $[10\bar{1}0]$ or $[1\bar{2}10]$ directions (Kelley and Hosford, 1967, 1968). These differences are attributed to the different lattice orientations in the two cases after twinning is complete (Kelley and Hosford, 1967) resulting in the activation of different slip modes. Such observations are significantly useful in prescribing realistic parameters for crystallographic slip and twin modes in the SCP models. In this work, we demonstrate that including the DT-induced lattice reorientation is important in order to highlight these differences that arise due to the activation of different slip activities after twinning is complete. Although not

[5] With Burgers vector $\langle a \rangle$, i.e. the slip direction $\boldsymbol{s} = (1/3)11\bar{2}0$.

Please cite this article as: Zhang, J., Joshi, S.P., Phenomenological crystal plasticity modeling and detailed micromechanical investigations of pure magnesium. J. Mech. Phys. Solids (2012), doi:10.1016/j.jmps.2012.01.005

Table 1
Slip and twin systems in Mg considered in the present work.

	Slip/twin plane	Slip direction/shear direction by twinning	Number of systems	Amount of shear
Basal	(0001)	$\langle 11\bar{2}0\rangle$	3	–
Prismatic	$\{10\bar{1}0\}$	$\langle 11\bar{2}0\rangle$	3	–
Pyramidal $\langle a\rangle$	$\{10\bar{1}1\}$	$\langle 11\bar{2}0\rangle$	6	–
Pyramidal $\langle c+a\rangle$	$\{10\bar{2}2\}$	$\langle 11\bar{2}3\rangle$	6	–
Tension twin (TT)	$\{10\bar{1}2\}$	$\langle 11\bar{1}1\rangle$	6	0.129
Compression twin (CT)	$\{10\bar{1}1\}$	$\langle 11\bar{1}\bar{2}\rangle$	6	0.138

discussed in this paper in detail, texture evolution in polycrystals also has important contributions from the DT-induced lattice reorientation (e.g. Clausen et al., 2008).

The aforementioned observations provide some useful insight into the rich deformation mechanisms in Mg that need to be accounted for within the SCP framework. Therefore, we include the crystallographic descriptions of the basal, prismatic, pyramidal $\langle a\rangle$ and pyramidal $\langle c+a\rangle$ slip, the $\{10\bar{1}2\}\langle\bar{1}011\rangle$ TT mode and the $\{10\bar{1}1\}\langle 10\bar{1}\bar{2}\rangle$ CT mode in describing the constitutive behavior of Mg single crystals (Table 1 and Fig. 1).

2.2. Rate-dependent SCP model for Mg

The spatial velocity gradient $\mathbf{L}$ is assumed to be composed of the elastic velocity gradient $\mathbf{L}^e$ and the plastic velocity gradient $\mathbf{L}^p$[6] :

$$\mathbf{L}=\dot{\mathbf{F}}\mathbf{F}^{-1}=\mathbf{L}^e+\mathbf{L}^p \tag{1}$$

where, $\dot{\mathbf{F}}$ and $\mathbf{F}^{-1}$ are the material derivative and inverse of the deformation gradient $\mathbf{F}$. Motivated by Kalidindi (1998), the constitutive law for the plastic velocity gradient is assumed to have contributions from slip in the parent (i.e. untwinned region), twinning in the parent region, and slip in the twinned region[7] :

$$L^p=\underbrace{\left(1-\sum_{\beta}^{N_{tw}}f^{\beta}\right)\sum_{\alpha=1}^{N_s}\dot{\gamma}^{\alpha}(\mathbf{s}^{*(\alpha)}\otimes\mathbf{m}^{*(\alpha)})}_{\text{slip in parent}}+\underbrace{\sum_{\beta=1}^{N_{tw}}\dot{\gamma}^{\beta}(\mathbf{s}^{*(\beta)}\otimes\mathbf{m}^{*(\beta)})}_{\text{twinning in parent}}+\underbrace{\sum_{\beta=1}^{N_{tw}}f^{\beta}\sum_{\tilde{\alpha}=1}^{N_s}\dot{\gamma}^{(\tilde{\alpha})}(\mathbf{s}^{*(\tilde{\alpha})}\otimes\mathbf{m}^{*(\tilde{\alpha})})}_{\text{slip in twinned region}} \tag{2}$$

where $\dot{\gamma}^{\alpha}$ denotes the shear rate on the αth slip system, f^{β} and $\dot{\gamma}^{\beta}$, respectively, denote the current twin v.f. and shear strain rate due to twinning (from the nucleation of new twins and growth of existing twins). Note that the initial (i.e. at time $t=0$) twin v.f. f_0^{β} corresponding to each twin system may be non-zero, indicating an initial twin population. N_s and N_{tw} denote the total number of slip and twin systems, respectively, $\mathbf{m}^*$ is the slip/twin plane normal vector and $\mathbf{s}^*$ is the corresponding slip/twin direction vector. The average Cauchy stress tensor $\boldsymbol{\sigma}$, at each material point due to twinned and parent regions is

$$\boldsymbol{\sigma}=\left(1-\sum_{\beta=1}^{N_{tw}}f^{\beta}\right)\boldsymbol{\sigma}^{m}+\sum_{\beta=1}^{N_{tw}}f^{\beta}\boldsymbol{\sigma}^{tw(\beta)} \tag{3}$$

2.2.1. Constitutive law for crystallographic slip

The slip rate for αth slip system within the parent region or $\tilde{\alpha}$th slip system within the twinned region[8] in Eq. (2) is assumed to follow a power-law[9]

$$\dot{\gamma}^{i}=\dot{\gamma}_0\left|\frac{\tau^i}{g^i}\right|^m sgn(\tau^i)\ (i=\alpha \text{ or } \tilde{\alpha}) \tag{4}$$

where $\dot{\gamma}_0$ is the reference slip rate assumed here to be the same for all the slip systems,m is the rate-sensitivity exponent for slip evolution and $\tau^i=\mathbf{m}^{*(i)}\cdot\boldsymbol{\sigma}\cdot\mathbf{s}^{*(i)}$ is the local resolved shear stress (RSS). The current slip system strength g^i is given as

$$g^i=\tau_0^i+\int_{t_0}^{t_1}\dot{g}^i_{sl\leftrightarrow sl}\,dt+\int_{t_0}^{t_1}\dot{g}^i_{tw\rightarrow sl}\,dt \tag{5}$$

[6] Throughout the text, uppercase bold Latin and bold Greek alphabets refer to second-order tensors, while lowercase bold Latin alphabets indicate first-order tensors. Italicized, plain Greek and Latin variables denote scalar components.

[7] $\tilde{\alpha}$ is related to α via $\mathbf{R}^{tw}$ (Eq. (26)).

[8] We denote individual slip systems by the lowercase Greek letter α or $\tilde{\alpha}$ and twin systems by β.

[9] Throughout the paper, a quantity with an over-dot indicates time derivative.

Please cite this article as: Zhang, J., Joshi, S.P., Phenomenological crystal plasticity modeling and detailed micromechanical investigations of pure magnesium. J. Mech. Phys. Solids (2012), doi:10.1016/j.jmps.2012.01.005

where τ_0^i is the initial ($t_0=0$) strength (CRSS) for ith slip system, $\dot{g}^i_{sl\leftrightarrow sl}$ and $\dot{g}^i_{tw\rightarrow sl}$ give the hardening rates of the slip system due to slip–slip and twin–slip interactions, respectively. Firstly, the hardening due to slip–slip interaction is discussed and the interactions between twin and slip are deferred until Sections 2.3 and 2.4.

The evolution of slip resistance on ith family of slip system due to slip–slip interaction is described in a conventional manner as

$$\dot{g}^i_{sl\leftrightarrow sl}=\sum_{j=1}^{N_s} h_{ij}(\overline{\gamma})\dot{\gamma}^j \tag{6}$$

where N_s is the number of slip systems, h_{ij} are the self ($i=j$) and latent ($i\neq j$) hardening moduli that depend on the total shear strain accumulated due to the slip in a given region (i.e. either in the parent or twinned regions)

$$\overline{\gamma}=\sum_{i=1}^{N_s}\int_{t_0}^{t}|\dot{\gamma}^i|dt \tag{7}$$

It is further assumed that

$$\begin{aligned} &h_{ii}=h(\overline{\gamma}) \quad \text{(no sum on } i\text{)}\\ &h_{ij}=qh(\overline{\gamma}) \quad (i\neq j)\end{aligned} \tag{8}$$

where $q\sim 1$–2 signifies latent hardening. For the non-basal slip modes we employ a hyperbolic hardening function (Peirce et al., 1982):

$$h(\overline{\gamma})=h_0\,\mathrm{sech}^2\left|\frac{h_0(\overline{\gamma})}{\tau_s^\alpha-\tau_0^\alpha}\right| \tag{9}$$

where τ_s^α is the saturation stress and h_0 is the initial hardening modulus. In accordance with experiments (e.g. Lavrentev and Pokhil, 1975), the basal slip is assumed to follow linear hardening

$$h(\overline{\gamma})=h_0 \tag{10}$$

Although discussed later in detail (Sections 2.3.3, 2.4.1, and 2.4.2), the possible *latent* hardening between the slip and twin systems in Mg may be briefly summarized in two ways (i) how slip affects twin evolution: the slip–twin interaction ($g_{sl\rightarrow tw}$) and (ii) how twin evolution affects slip: the twin–slip interaction ($g_{tw\rightarrow sl}$).

2.3. Evolution of twin volume fraction and DT-induced hardening

The contribution from DT to overall hardening behavior of Mg is a problem that has not been resolved fully yet, but within SCP it must be related to the manner in which twin v.f.'s evolve. To this end, it is important to note that the evolution characteristics of TT and CT differ substantially in Mg:

1. CTs are difficult to occur due to their high CRSS. When formed, they manifest as thin bands (Kelley and Hosford, 1968; Kitahara et al., 2007; Nave and Barnett, 2004; Yoshinaga et al., 1973), which is connected to the sessile nature of its dislocations that have a very narrow core width (Christian and Mahajan, 1995; Serra et al., 1991). The total CT v.f., f_{ct}, is usually much smaller compared to its tensile counterparts (Barnett, 2007), which is consistent with the notion of the difficulty associated with their nucleation and growth. Consequently, a CT may act as a barrier to dislocations, which may play a very effective role in strain hardening not only in Mg alloys (Knezevic et al., 2010) but also in pure Mg by restricting the slip length. Moreover, $\{10\bar{1}1\}$–$\{10\bar{1}2\}$ double twinning (Barnett et al., 2008; Crocker, 1962; Hartt and Reed-Hill, 1968; Ma et al., 2011; Yoshinaga et al., 1973) is frequently observed under the c-axis compression. Experimental observations (Barnett, 2007; Hartt and Reed-Hill, 1968) indicate that a double twinned region is plastically softer and exhibits large strain accumulation than the surrounding matrix rendering it a potential site for crack nucleation that affects the overall ductility. The large strain accumulation could be one reason why their twin boundaries (TBs) may not be able to migrate as easily as their tensile partners, resulting in thin CT bands. Moreover, Knezevic et al. (2010) also indicate that the extension twin inside of the CT will inhibit thickening of this double twin by loss of twin-matrix conherency.
2. The CRSS for tensile twins (TT) nucleation is much lower than that for CT. Further, unlike CTs, TTs evolve much more rapidly through nucleation and TB migration.

2.3.1. Twin nucleation and propagation resistance

The evolution of DT (TT and CT) v.f. involves nucleation of new twins and growth of existing ones and the resistance to their evolution comes from the twin–twin and slip–twin interactions. The twin–twin interaction process including intersection of twins, the formation of twins and so on (Yoo, 1981), may feature very complex mechanisms. In the present SCP framework, we do not handle discrete twins. Instead their collective behavior is incorporated as a twin v.f. that evolves with deformation. Therefore, the resistance to twin evolution needs to be appropriately embedded within its constitutive description. The plastic shearing rate $\dot{\gamma}^\beta$ due to twinning of βth twin system is related to the twin v.f. evolution $\dot{f}$ via

Please cite this article as: Zhang, J., Joshi, S.P., Phenomenological crystal plasticity modeling and detailed micromechanical investigations of pure magnesium. J. Mech. Phys. Solids (2012), doi:10.1016/j.jmps.2012.01.005

constant twinning shear γ^{tw} (Hosford, 1993):

$$\dot{\gamma}^{\beta} = \dot{f}^{\beta}\gamma^{tw} \tag{11}$$

where

$$\gamma^{tw} = \begin{cases} \gamma_{tt}^{tw} = \frac{\sqrt{3}}{\chi} - \frac{\chi}{\sqrt{3}} & \{10\bar{1}2\} \quad \text{(tensile mode)} \\ \gamma_{ct}^{tw} = \frac{4\chi^2 - 9}{4\sqrt{3}\chi} & \{10\bar{1}1\} \quad \text{(compressive mode)} \end{cases} \tag{12}$$

and $\chi = c/a = 1.624$ for Mg. In its present form, Eq. (11) does not account for elastic twins (Boiko et al., 1994) and stopped elastic twins (Marshall and McLaren, 1977).[10] Noting again that the evolution of twin v.f. must account for nucleation of new twins $\dot{f}_n$, and growth of existing twins $\dot{f}_g$, irrespective of the twin type, we write,

$$\dot{f}^{\beta} = \dot{f}^{\beta}{}_n + \dot{f}_g^{\beta} \tag{13}$$

If we assume that twin evolution follows Schmid law (Brown et al., 2005; Park et al., 2010) and that a power-law form is appropriate for both components of twin fraction, then[11]

$$\dot{f}^{\beta} = \underbrace{\dot{f}_{0\_n}(\tau^{\beta}/s_{tw\_n}^{\beta})^{m_t}}_{\dot{f}_n^{\beta}} + \underbrace{\dot{f}_{0\_g}(\tau^{\beta}/s_{tw\_g}^{\beta})^{m_t}}_{\dot{f}_g^{\beta}} \tag{14}$$

where $s_{tw\_n}^{\beta}$ and $s_{tw\_g}^{\beta}$ are, respectively, the current twin system strengths corresponding to nucleation and growth and governed by the twin–twin and slip–twin interactions, m_t is the rate-sensitivity exponent for twinning and $\dot{f}_{0\_}n$ and $\dot{f}_{0\_g}$ are the reference v.f. evolution rate for twin nucleation and growth, respectively. While the functional form of Eq. (14) is applicable to the TTs and CTs alike, presently it is difficult to obtain descriptions of these evolutionary parameters because (a) the nucleation and growth processes are difficult to isolate in experiments, and (b) the evolution characteristics are different in TTs and CTs (Section 2.3). In the absence of such information, we make simplifying assumptions on Eq. (14) by assuming that for a given twin type (i.e. TT or CT) the average reference nucleation and growth rates are the same, but are modulated by appropriate hardening functions. This is an ad hoc assumption, but it helps retain the distinction between the CT and TT characteristics.

The lethargy of the CT for initial nucleation may be incorporated through a high CRSS for the CT systems. For βth CT system, the CT v.f. evolution may be written as

$$\dot{f}_{ct}^{\beta} = \dot{\bar{f}}_{0\_ct}\left(\frac{\tau^{\beta}}{s_{ct}^{\beta}}\right)^{m_t} \tag{15}$$

where s_{ct}^{β} is its current total CT system resistance (discussed further in Section 2.3.2), τ^{β} is the RSS, $\dot{\bar{f}}_{0\_ct} = \dot{\gamma}_0^{ct}/\gamma_{ct}^{tw}$ is the average reference CT v.f. evolution rate and m_t is the rate-sensitivity exponent. From a polycrystal Mg observation (Barnett, 2007) the total CT v.f. at a nominal strain $\sim$10% is about 5% giving an approximate CT v.f. evolution rate $\sim 10^{-4}\,s^{-1}$.

On the other hand, nucleation of TTs is relatively easy and once formed they also grow rapidly. In essence, both the contributions are deemed equally important in the evolution of TT v.f. and therefore, we may again assume a single function that combines the two contributions

$$\dot{f}_{tt}^{\beta} = \dot{\bar{f}}_{0\_tt}\left(\frac{\tau^{\beta}}{s_{tt}^{\beta}}\right)^{m_t} \tag{16}$$

where s_{tt}^{β} is the current resistance strength for TT evolution (Section 2.3.2) and $\dot{\bar{f}}_{0\_tt}$ is the average reference twin v.f. increment rate, $\dot{\bar{f}}_{0\_tt} = \dot{\gamma}_0^{tt}/\gamma_{tt}^{tw}$. Experiments indicate that $\dot{\bar{f}}_{0\_tt} = 10^{-2}-10^{-3}\,s^{-1}$, which is at least an order of magnitude higher than its compressive counterpart.

2.3.2. Evolution of twin–twin interaction($\dot{s}_{tw\leftrightarrow tw}^{\beta}$):

Irrespective of CT or TT, the current strength s^{β}(*i.e.*s_{ct}^{β} and s_{tt}^{β}) of βth twin system (Eqs. (15) and (16)) may in general be written as

$$s^{\beta} = \tau_0^{\beta} + \int_{t_0}^{t_1}(\dot{s}_{tw\leftrightarrow tw}^{\beta} + \dot{s}_{sl\rightarrow tw}^{\beta})dt \tag{17}$$

where τ_0^{β} is the appropriate (TT or CT) CRSS(t_0=0), $\dot{s}_{tw\leftrightarrow tw}^{\beta}$and $\dot{s}_{sl\rightarrow tw}^{\beta}$, respectively, describe the hardening due to twin–twin and slip–twin interactions (compare Eq. (5)), for the TTs and CTs, elaborated next. The twin–twin interaction may be due to (a) twin intersection, i.e. twins crossing other twins (Cahn, 1953), (b) the Hall–Petch type behavior (Yu et al., 2010), and/or (c) double twinning. While the first aspect may be true in both, CTs and TTs, the latter factors are likely relevant only in

[10] We acknowledge one of the reviewers for this point.

[11] Very recently, Beyerlein and co-workers (Beyerlein et al., 2010; Beyerlein and Tomé, 2010) have proposed a probabilistic theory for twin nucleation in HCP polycrystals to address non-Schmid effects.

Please cite this article as: Zhang, J., Joshi, S.P., Phenomenological crystal plasticity modeling and detailed micromechanical investigations of pure magnesium. J. Mech. Phys. Solids (2012), doi:10.1016/j.jmps.2012.01.005

the case of CTs. Although the mechanisms for either situation may be different, they may both result in impeding the twin evolution process. (Cahn, 1953; Christian and Mahajan, 1995; Yoo, 1981).

Resistance to CT v.f. evolution may be attributed to several different mechanisms. Low mobility of CT dislocations emanating from their narrow core-width (Christian and Mahajan, 1995; Serra et al., 1991) is likely to cause sluggish CT growth. This may result in thin CT morphologies within a grain that may in turn resist nucleation of new twins a lá Hall–Petch behavior. Kalidindi (2001) favored this argument, albeit in the context of slip hardening due to twinning (see Section 2.4.1), but it may also be valid for CT system hardening. Double twinning in existing twins may also resist their further growth (Hartt and Reed-Hill, 1968). To account for these mechanisms (Eq. (17)), we propose the following evolution law for twin–twin interaction hardening of βth CT system

$$\dot{s}^{\beta}_{ct\leftrightarrow ct}=\left(\underbrace{H_{ct-n}\left(\sum_{m=1}^{N_{ct}}f^{m}\right)^{-0.5}}_{\substack{\text{resistance to CT nucleation}\\ \text{from existing CTs}}}+\underbrace{H_{ct-g}\left(\sum_{m=1}^{N_{ct}}f^{m}\right)^{k}}_{\substack{\text{resistance to growth}\\ \text{of existing CTs}}}\right)\dot{\gamma}^{\beta} \tag{18}$$

where $\sum_{m=1}^{N_{ct}}f^{m}$ is the current total v.f. on N_{ct} CT systems, H_{ct-n} is the Hall–Petch type material hardening parameter. The coefficients H_{ct-g} and k account for the resistance to propagation due to double twinning and low twin dislocation mobility. It is assumed that the TT v.f. inside the CTs is tied to the evolution of CT v.f. Noting that both the terms in Eq. (18) are related to CT v.f., we choose to simplify it by assuming a single function that approximately combines the two contributions

$$\dot{s}^{\beta}_{ct\leftrightarrow ct}=H_{ct}\left(\sum_{m=1}^{N_{ct}}f^{m}\right)^{b}\dot{\gamma}^{\beta} \tag{19}$$

where H_{ct} and b control the hardening rate of CT systems. Although such an approximation does not retain the original structure of Eq. (18), it allows us reducing the number of free parameters, yet capture the assumed physics of the hardening evolution in an average sense through an appropriate choice of H_{ct} and b. We note that the functional form of Eq. (19) bears similarity to that proposed by Salem et al. (2005) who described the twin–twin interaction in titanium ($\alpha-$Ti); however, there are a couple of important differences to be noted. Firstly, they adopted a high value for $b(\sim 10)$ together with a very high hardening parameter ($\sim$100 GPa) to mimic the twin v.f. evolution in $\alpha-$Ti. Secondly, in our case Eq. (19) is assumed to be applicable only for the CTs as their evolution characteristics are distinct from TT; Salem et al. (2005) did not distinguish between them in the case of $\alpha-$Ti as it may not be important there. To model the sluggish kinetics of CT evolution at early strains, we adopt $b\ll 1$ and H_{ct} that is in the range of few GPa (Table 3). Although these values are by no means unique they provide consistent corroboration with experiments (Barnett, 2007; Hartt and Reed-Hill, 1968) in terms of CT evolution. Kalidindi (2001) adopted a similar argument to model twinning kinetics in low stacking fault energy FCC crystals. In the case of Mg the choice of b and H_{ct} ascribes this sluggishness to a high hardening rate, attributed to resistance to CT from the aforementioned mechanisms (Barnett, 2007; Kitahara et al., 2007, also see Sections 2.3, no. 1).

Unlike CTs, the propensity of TTs to easy nucleation and growth stems from high mobility of TT dislocations, due to a much larger dislocation core width that is nearly 3–6 times of their CT counterpart (Christian and Mahajan, 1995). Under favorable conditions TTs rapidly engulf parent region. Consequently, one could expect that such a process may result in a saturation type hardening, which can be represented by the form identical to the slip system hardening. There is also some experimental evidence of such a behavior in single-crystal (Kelley and Hosford, 1968) and polycrystalline Mg (Li and Enoki, 2007). Therefore, evolution of the hardening for βth TT system due to twin–twin interaction (Eq. (17)) reads (similar to the slip system hardening)

$$\dot{s}^{\beta}_{tt\leftrightarrow tt}=\dot{s}^{\beta}_{tt}=h^{\beta}_{tt}\,\mathrm{sech}^{2}\left|\frac{h^{\beta}_{tt}\overline{\gamma}_{tt}}{\tau^{\beta}_{s-tt}-\tau^{\beta}_{0-tt}}\right|\dot{\gamma}^{\beta} \tag{20}$$

where h^{β}_{tt} is the initial hardening for βth TT system, τ^{β}_{0-tt} and τ^{β}_{s-tt} are, respectively, the CRSS and saturation stress for that TT system and $\overline{\gamma}_{tt}$ is the accumulated shear strain on all TT systems.

Although twinning is modeled here as pseudo-slip that relies on Schmid law (Christian and Mahajan, 1995) only the positive RSS (i.e. concomitant with the twinning direction) is allowed to accrue plastic strain in order to mimic the polar[12] nature of twinning. Therefore, Eqs. (15) and (16) are also subject to the following constraints:

$$\dot{f}^{\beta}>0,\ \sum_{\beta=1}^{N_{tw}}f^{\beta}\le f_{cr} \tag{21}$$

[12] Unlike plastic slip that may occur in either direction of the slip vector, twinning is strongly biased to occur in one direction only on a given twin plane. De-twinning is possible, but neglected here for simplicity.

Please cite this article as: Zhang, J., Joshi, S.P., Phenomenological crystal plasticity modeling and detailed micromechanical investigations of pure magnesium. J. Mech. Phys. Solids (2012), doi:10.1016/j.jmps.2012.01.005

where f_{cr} denotes the critical twin v.f. at which the lattice reorientation scheme is invoked at a material point. We discuss the DT induced lattice reorientation in Section 2.5.

2.3.3. Effect of slip on CT and TT evolution ($\dot{\boldsymbol{s}}_{\boldsymbol{sl\rightarrow tw}}$)

The evolution of the hardening of twin systems due to their interaction with the slip systems (Eq. (17)) poses interesting questions in terms of the interaction of twins with dislocation slip: How do slip systems influence twin system hardening? Does twinning become increasingly difficult if it were preceded by slip (i.e. s^{β} evolves with dislocation slip preceding twinning) or does twinning occur independently of the slip-induced hardening (i.e. $s^{\beta}=\tau_0^{\beta}$, if $\tau^{\beta}<\tau_0^{\beta}$)? Are these interactions different in CTs and TTs? While there are no clear observations related to the effect of slip on CT evolution in Mg, a recent study on Zr (Capolungo et al., 2009a) indicates that at least the onset of CT is insensitive to the stored dislocation density. Also, a *slip-independent* TT evolution has been postulated in Mg (Capolungo et al., 2009b). This is a topic that needs some fundamental experimental investigations, because different types of dislocations (i.e. prismatic, pyramidal, and so on) may interact differently with TBs (Capolungo et al., 2009b) and this intricate aspect requires detailed calculations at finer length-scales (e.g. MD) before integrating more detailed information into SCP frameworks. In the wake of aforementioned observations, we assume a slip-independent latent hardening for TTs and CTs, i.e. $\dot{s}_{sl\rightarrow tw}=0$. We demonstrate later that this assumption may be a possible reason for the orientation-dependent occurrence of CT under *c*-axis compression.

2.4. Effect of CT and TT on slip hardening evolution ($\dot{\boldsymbol{g}}_{\boldsymbol{tw\rightarrow sl}}$)

The slip system hardening due to DT has been ascribed to different mechanisms: (1) the Hall–Petch effect (Capolungo et al., 2009a; Kalidindi, 2001; Knezevic et al., 2010), where the TBs act as barriers to dislocation motion in the matrix or within twins, more likely to be applicable for CTs given their thin structure in Mg, (2) transmutation mechanism (El Kadiri and Oppedal, 2010) in that the initially glissile dislocations in the matrix become sessile as a result of the twinning shear transformation, (3) twinning accommodation effect (Christian and Mahajan, 1995; EI Kadiri and Oppedal, 2010; Roberts and Partridge, 1966), wherein slip dislocations are emitted to accommodate the shape changes near twinning boundaries in matrix and within the twins or (4) texture hardening mechanism due to the twinning-induced lattice reorientation, likely a more relevant mechanism for TT rather than CT.[13] On this backdrop, it is important to distinguish the roles that the CTs and TTs play as they interact with dislocation slip contributing to the latent slip hardening. Based on these arguments we now prescribe how $g^{\beta}_{tw\rightarrow sl}$ (Eq. (5)) evolves in the presence of twin v.f.

2.4.1. CT–slip interaction

Given that a typical CT in Mg is a thin, long band that divides a grain into smaller regions, the length of slip dislocation is reduced. This can cause an increase in hardening of slip systems in the matrix regions. Therefore, the effect of twinning to slip could be mainly described as a Hall–Petch (H–P) type relationship (Kalidindi, 2001). Assuming an array of parallel CTs of equal thickness (Remy, 1978), the average twinning spacing t is proportional to the reciprocal of the CT v.f. f_{ct}. This t may be treated as the *modified* grain size to account for the effect of twinning to slip via H–P relationship. Therefore, the contribution to the overall hardening of αth slip system from CT–slip interaction assumes a Taylor-hardening type form that depends on the total v.f. accumulated over all the N_{ct} CT systems

$$g^{\alpha}_{ct\rightarrow sl}=H_{ct\rightarrow sl}\left(\sum_{\beta=1}^{N_{ct}} f^{\beta}_{ct}/\gamma^{tw}_{ct}\right)^{0.5}=H_{ct\rightarrow sl}(\overline{\gamma}_{ct})^{0.5} \tag{22}$$

and the corresponding evolution law becomes

$$\dot{g}^{\alpha}_{ct\rightarrow sl}=0.5H_{ct\rightarrow sl}(\overline{\gamma}_{ct})^{-0.5}\dot{\overline{\gamma}}_{ct} \tag{23}$$

where $H_{ct\rightarrow sl}$ represents the initial material hardening parameter for the CT–slip interaction. Eq. (23) denotes the collective effect of all the CT systems on the hardening rate of slip system α.

2.4.2. TT–slip interaction

As discussed previously, unlike CTs, TTs evolve rapidly and their TBs move quickly; therefore, the H–P relationship may not be applicable for TT–slip interaction (El Kadiri and Oppedal, 2010). The TT–slip interaction is also captured partly by the texture hardening mechanism automatically through DT-induced lattice-reorientation (Section 2.5.1). Due to possible hardening mechanisms, as the tensile twinning shows the saturation type of evolution, we incorporate a saturation-type hardening law (similar to Eq. (20)) for the TT–slip interaction

$$\dot{g}^{\alpha}_{tt\rightarrow sl}=h_{tt\rightarrow sl}\,\mathrm{sech}^2\left|\frac{h_{tt\rightarrow sl}\overline{\gamma}_{tt}}{\tau^{\beta}_{s-tt}-\tau^{\beta}_{0-tt}}\right|\dot{\gamma}^{\beta} \tag{24}$$

where $h_{tt\rightarrow sl}$ is the latent hardening parameter describing the TT–slip interaction.

[13] It is observed that CT does not contribute significantly to overall texture changes (Brown et al., 2005; Nave and Barnett, 2004).

Please cite this article as: Zhang, J., Joshi, S.P., Phenomenological crystal plasticity modeling and detailed micromechanical investigations of pure magnesium. J. Mech. Phys. Solids (2012), doi:10.1016/j.jmps.2012.01.005

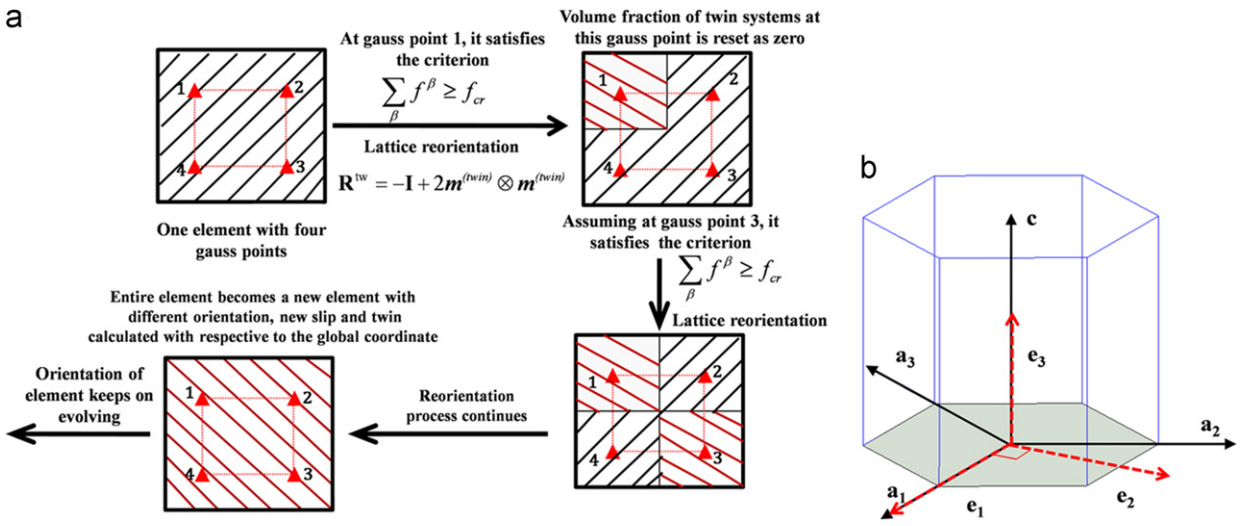

Fig. 3. (a) Schematic illustration of the DT-induced reorientation process with a single finite element and (b) relation between the 3-axis and 4-axis coordinate system for an HCP lattice.

The kinematics and kinetics of crystallographic slip and twin modes explained in Sections 2.2–2.4 is implemented in ABAQUS/STANDARD as a user-material subroutine (UMAT).

2.5. Numerical implementation of lattice reorientation

2.5.1. DT-induced lattice reorientation:

There are two important aspects of twinning that need to be included in the finite element (FE) implementation of the SCP framework: (i) the evolution of twin population and (ii) lattice reorientation. Eqs. (15) and (16) track twin v.f. evolution on each twin system that are evaluated at each material point (or each Gauss point (GP) in the FE context). When twinning is absent, $\sum_{\beta=1}^{N_{tw}} f^\beta = 0$. Fig. 3a shows the lattice reorientation scheme applied within an individual FE. At a GP, when the total twin v.f. on all the twin systems ($\sum_{\beta=1}^{N_{tw}} f^\beta$) reaches a certain critical value, f_{cr}, the volume represented by that GP is rotated from its original orientation to the twinned one.

The new lattice orientation is determined by the twin system that has the highest contribution to the total twin v.f. The changes in the twin v.f. at each GP are updated at the end of each strain increment. We adopt a three-axis instead of the four-axis basis to define the reorientation scheme (Fig. 3b). The transformation between the original (e_i) and new ($\boldsymbol{e}_i^R$) lattice base vectors is given by

$$\mathbf{e}_i^R = \mathbf{R}^{tw}\mathbf{e}_i \tag{25}$$

where $\mathbf{R}^{tw}$ is the rotation tensor due to twinning (Christian and Mahajan, 1995)

$$\mathbf{R}^{tw} = -\mathbf{I} + 2\mathbf{m}^{tw} \otimes \mathbf{m}^{tw} \tag{26}$$

with $\mathbf{I}$ being the identity tensor and $\mathbf{m}^{tw}$ defining the twinning plane normal. After reorientation, the twin v.f. on each twin system is reset to zero and the RSS on the reoriented systems is re-calculated.

2.5.2. Spin induced lattice reorientation

Besides DT-induced lattice reorientation, the crystal lattice also undergoes elastic rotation as the deformation progresses. The elastic lattice rotation affects the reciprocal vectors coinciding with the slip [twin] directions, $\mathbf{s}^{*(\alpha)}[\mathbf{s}^{*(\beta)}]$, and the normals to the slip [twin] planes, $\mathbf{m}^{*(\alpha)}[\mathbf{m}^{*(\beta)}]$, in the deformed configuration. The changes in the orientation of $\mathbf{s}^*$ and the normal $\mathbf{m}^*$ due to the elastic rotation of the crystal lattice are accounted for via the elastic spin tensor $\boldsymbol{\Omega}^e$

$$\begin{aligned} \dot{\mathbf{s}}^{*(\alpha,\beta)} &= \boldsymbol{\Omega}^e \cdot \mathbf{s}^{*(\alpha,\beta)} \\ \dot{\mathbf{m}}^{*(\alpha,\beta)} &= -\boldsymbol{\Omega}^e \cdot \mathbf{m}^{*(\alpha,\beta)} \end{aligned} \tag{27}$$

where

$$\boldsymbol{\Omega}^e = \tfrac{1}{2}(\mathbf{L}^e - (\mathbf{L}^e)^T) \tag{28}$$

Then, $\mathbf{s}^*$ and $\mathbf{m}^*$ are updated at each time step.

Please cite this article as: Zhang, J., Joshi, S.P., Phenomenological crystal plasticity modeling and detailed micromechanical investigations of pure magnesium. J. Mech. Phys. Solids (2012), doi:10.1016/j.jmps.2012.01.005

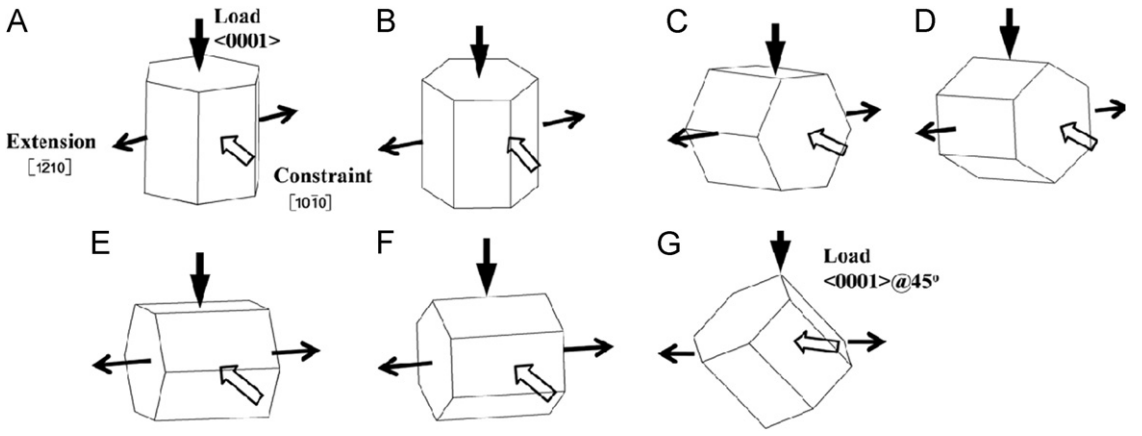

Fig. 4. Single crystal orientations considered in plane-strain compression simulations (Kelley and Hosford, 1967, 1968).

Table 2
Elastic constants (MPa) for pure Mg single crystal at 300 K.

C11	C12	C13	C33	C44
59,400	25,610	21,440	61,600	16,400

3. Crystal-plasticity model simulations and discussion

In an elaborate set of experimental investigation, K–H (Kelley and Hosford, 1967) performed plane-strain compression on pure Mg single crystals at room temperature for seven different crystal orientations (Fig. 4a–g). In the figure, a thick solid arrow indicates the direction of loading, a thin solid arrow indicates extension direction and an open arrow indicates the constraint direction. For this work, we first established the parameters in the constitutive equations by modeling these orientations and carefully corroborating the macroscopic and microscopic responses with K–H experiments.

3.1. Constitutive parameters for Mg single crystals

Table 2 gives the elastic constants used in the simulations (Long and Smith, 1957; Slutsky and Garland, 1957) and Table 3 summarizes key crystallographic slip and twin constitutive expressions together the final values adopted for the material parameters. The initial guesses for the CRSS values corresponding to the slip and twin systems were based on the ranges shown in Fig. 2. With repeated brute force trials critically comparing the simulations for different orientations with corresponding K–H results, final choice of parametric combinations were obtained. We do not elaborate the trial and error method here, but provide a brief account of the broad procedure adopted here. Basal slip was the easiest to calibrate which can be activated in isolation under orientation G (Fig. 4g). Orientations A and B correspond to a compressive loading along the c-axis that can be accommodated by pyramidal $\langle c+a \rangle$ slip and CT modes. In the Mg literature, measuring the CRSS for CT has been a persistent challenge, because the samples are prone to fracture with the onset of these twins. Therefore, many works simply ignore this twinning mode in their simulations while some others use the ultimate stress as an estimate to calculate the CRSS, which may be an over prediction. In this work, we fitted the constitutive parameters for the $\{10\bar{1}1\}$ CT using B orientation and predicted its activity for orientation A. Likewise, pyramidal $\langle c+a \rangle$ was calibrated for orientation A and predicted for orientation B. For both orientations, single crystal experiments unequivocally report the latter indicating that it is likely a preferred mechanism over the former. Orientations C and D favor the $\{10\bar{1}0\}\langle 11\bar{2}0 \rangle$ prismatic and $\{10\bar{1}1\}\langle 11\bar{2}0 \rangle$ pyramidal slip systems, and we calibrated their constitutive parameters using these orientations. The E and F orientations favor $\{10\bar{1}2\}$ TT; the Schmid factors for the TT systems are 0.5 (case E) and 0.37 (case F). Therefore, the model constitutive parameters for TT including the CRSS, hardening and the critical strain, ε_c, corresponding to complete twinning ($\sim$6%) were calibrated with case E and predicted for case F. In the next section, we provide a detailed account of the final observations vis-à-vis experiments (primarily K–H, but also includes other similar experimental observations) pertaining to the macroscopic stress–strain behaviors and corresponding microscopic slip and twin evolution.

3.2. Plane-strain compression of single-crystal pure Mg: critical comparison with K–H experiments

It should be noted in plane-strain compression the RSS is calculated not only from the applied stress but also from the stress induced due to the constraint. In the simulations, we employed 3D finite elements (C3D8) for the specimens and

Please cite this article as: Zhang, J., Joshi, S.P., Phenomenological crystal plasticity modeling and detailed micromechanical investigations of pure magnesium. J. Mech. Phys. Solids (2012), doi:10.1016/j.jmps.2012.01.005

Table 3
Key slip and twin constitutive equations and calibrated parameters using (Kelley and Hosford, 1968, 1967) (stresses are in MPa).

Constitutive equations		Parameters			
Slip					
$\dot{\gamma}^i = \dot{\gamma}_0 \left\lvert \frac{\tau^i}{g^i} \right\rvert^m sgn(\tau^i)(i=\alpha \text{ or } \tilde{\alpha})$	(4)	$\dot{\gamma}_0 = 1\times10^{-3}s^{-1}, m=50$			
$g^i = \tau_0^i + \int_{t_0}^{t_1} \dot{g}^i_{sl\leftrightarrow sl}\,dt + \int_{t_0}^{t_1} \dot{g}^i_{tw\to sl}\,dt$	(5)	Basal	Prism	Pyr $\langle a \rangle$	Pyr $\langle c+a \rangle$
		τ_0 0.5	25	25	40
$\dot{g}^i_{sl\leftrightarrow sl} = \sum_{j=1}^{N_s} h_{ij}(\overline{\gamma})\dot{\gamma}^j$	(6)				
$h_{ii} = h(\overline{\gamma})$ (no sum on i) $h_{ij} = qh(\overline{\gamma})$ $(i\neq j)$	(8)			$q=1$	
$h(\overline{\gamma}) = h_0 \,\mathrm{sech}^2\left\lvert \frac{h_0\overline{\gamma}}{\tau_s^2-\tau_0^2} \right\rvert$ (non-basal slip)	(9)			h_0	τ_s
			Prism	1500	85
			Pyr $\langle a \rangle$	1500	85
			Pyr $\langle c+a \rangle$	3000	150
$h(\overline{\gamma}) = h_0$ (basal slip)	(10)	h_0=20			
Twin					
$\dot{\gamma}^\beta = \dot{f}^\beta \gamma^{tw}$	(11)				
CT					
$\dot{f} = \dot{f}^\beta_{ct} = \dot{\bar{f}}_{0\_ct}\left(\frac{\tau^\beta}{s^\beta_{ct}}\right)^{m_t}$	(15)	$\dot{f}_{0\_ct} = 1\times10^{-4}s^{-1}, m_t=50$			
TT					
$\dot{f} = \dot{f}^\beta_{tt} = \dot{\bar{f}}_{0\_tt}\left(\frac{\tau^\beta}{s^\beta_{tt}}\right)^{m_t}$	(16)	$\dot{f}_{0\_tt} = 1\times10^{-3}s^{-1}, m_t=50$			
$s^\beta = \tau_0^\beta + \int_{t_0}^{t_1}(\dot{s}^\beta_{tw\leftrightarrow tw} + \dot{s}^\beta_{sl\to tw})dt$	(17)				
CT					
$\dot{s}^\beta_{tw\leftrightarrow tw} = H_{ct}\left(\sum_{m=1}^{N_{ct}} f^m\right)^b \dot{\gamma}^\beta$	(19)	H_{ct}=6000, b=0.05, τ_{0-ct} =55			
TT					
$\dot{s}^\beta_{tw\leftrightarrow tw} = h^\beta_{tt}\,\mathrm{sech}^2\left\lvert \frac{h^\beta_{tt}\overline{\gamma}_{tt}}{\tau^\beta_{s-tt}-\tau^\beta_{0-tt}} \right\rvert \dot{\gamma}^\beta$	(20)	$h_{tt}=100$, $\tau_{s-tt}=20$, $\tau_{0-tt}=3.5$			
Twin–slip					
$\dot{g}^\alpha_{ct\to sl} = 0.5H_{ct\to sl}((\overline{\gamma})_{ct})^{-0.5}\dot{\overline{\gamma}}_{ct}$	(23)	$H_{ct\to sl}$=15			
$\dot{g}^\alpha_{tt\to sl} = h_{tt\to sl}\,\mathrm{sech}^2\left\lvert \frac{h_{tt\to sl}\overline{\gamma}_{tt}}{\tau^\beta_{s-tt}-\tau^\beta_{0-tt}} \right\rvert \dot{\gamma}^\beta$	(24)	$h_{tt\to sl}=h_{tt}$			

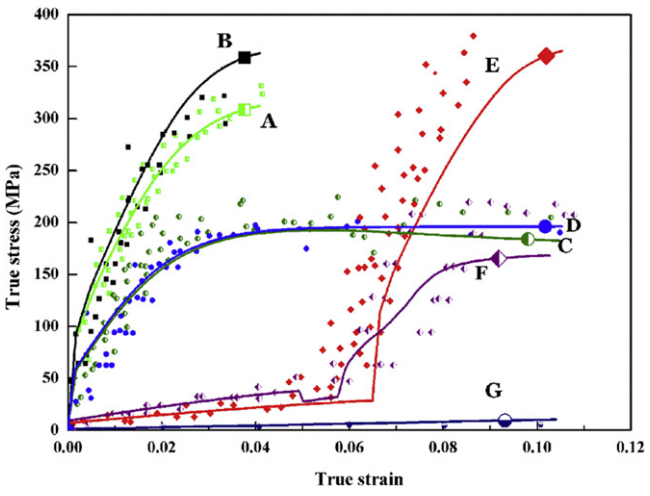

Fig. 5. Comparison of stress–strain responses from plane-strain compression simulations (solid lines) with K–H experiments (symbols). The raw experimental data are taken from Graff et al. (2007).

Please cite this article as: Zhang, J., Joshi, S.P., Phenomenological crystal plasticity modeling and detailed micromechanical investigations of pure magnesium. J. Mech. Phys. Solids (2012), doi:10.1016/j.jmps.2012.01.005

modeled the die-channel as a rigid wall. Fig. 5 shows the comparison between the K–H experimental average true stress–true strain $\sigma-\varepsilon$ data and our simulated results for the parameters presented in Table 3. The simulated macroscopic results compare well, capturing important trends for each orientation. Notably, the curves for the hardening rate $\theta=d\sigma/d\varepsilon$ as a function of stress σ also corroborate reasonably with the experimental hardening rates (Supplementary material A, Fig. A-1). However, as mentioned in the Introduction, we also critically corroborate the underlying microscopic deformation activities and relate them to these macroscopic responses. Therefore, we defined a measure $\bar{r}^{\alpha}$, defined as

$$\bar{r}^{\alpha}=\frac{1}{V}\int r^{\alpha}\,dv \tag{29}$$

where r^{α} is relative activity of the αth slip and twin mode at each material (Gauss) point, V is the total sample volume and dv is volume represented by a material point. For αth slip or twin mode, the relative activity r^{α} at each material point ($0\le r^{\alpha}\le 1$), is the ratio of the shear strain on that slip/twin system to the sum of the shear strain of all the slip and twin modes at a given time t in Eq. (30),

$$r^{\alpha}=\frac{\sum_{i=1}^{n}\xi_i|\Delta\gamma_i^{(\alpha)}|}{\sum_{\alpha=1}^{m}\sum_{i=1}^{n}\xi_i|\Delta\gamma_i^{(\alpha)}|},\quad \xi_i\begin{cases}=1-\sum_{\beta=1}^{N_{tw}}f^{\beta} & \text{(for slip in matrix)}\\ =1 & \text{(for twin in matrix)}\\ =f^{\beta} & \text{(for slip in twin)}\end{cases} \tag{30}$$

where $m(=6)$ is the total number of slip (4) and twin (2) modes, n is the number of slip/twin systems in a given mode (Table 1), f^{β} is the βth twin v.f. and $\Delta\gamma_i^{(\alpha)}$ is the plastic increment on the ith slip/twin system in the αth mode at time increment Δt. Fig. 6 shows the evolution of the relative activities of the various slips, and twin mechanisms with strain for each orientation. In the following sections, we discuss these results for each orientation in detail together with their corresponding macroscopic stress–strain responses.

3.2.1. Compression along the c-axis (cases A and B)

For the chosen material parameters, the predicted true stress–true strain curves for A and B (Fig. 5) closely agree with the experiments. Fig. 6a and b correspondingly shows that the pyramidal $\langle c+a\rangle$ is the dominant slip mode for both the orientations. In their report, K–H (Kelley and Hosford, 1967) remarked that the initial hardening up to 4% strain has contribution from the basal slip, but that is the case only because of the minor specimen misalignment in their experiments. In our simulations, we did not introduce any initial misalignment and therefore, no basal mode is activated and the compression is initially accommodated by pyramidal $\langle c+a\rangle$ mode (also see Graff et al., 2007; Capolungo et al., 2009b). Pyramidal $\langle c+a\rangle$ and CT are these two deformation modes accommodating the c-axis compression. Most Mg-related SCP simulations neglect the CT mode, but it has important influence on the failure and ductility of polycrystalline Mg (Agnew et al., 2006; Barnett, 2007), and therefore, should be included in a model:

a. Competition between pyramidal $\langle c+a\rangle$ and CT:
Kelley and Hosford (1967) experiments reported activation of CT for these orientations (also see Wonsiewicz, 1966). In our simulations, although the CRSS of the CT is larger than that of the pyramidal $\langle c+a\rangle$ mode, it is activated fairly early in both the cases, at a nominal strain $\sim$0.5%.Once the CTs are formed, they initially contribute to the total plastic strain causing a drop in the relative activity of the pyramidal $\langle c+a\rangle$ for a short duration. However, because the CT evolution is sluggish, the pyramidal activity picks up again, albeit gradually. This gradual increase is attributed to the hardening of the pyramidal system due to CT through the twin-slip interaction effect (Eqs. (22) and (23)) that supplements the slip–slip interaction that manifest as a strongly strain hardening response (Fig. 5a and b).
Fig. 6A and B also shows the predicted CT v.f. as a function of applied strain. For a nominal strain $\sim$4%, the overall CT v.f. is $\sim$0.08 for case A and $\sim$0.12 for case B. In literature, there is limited information available for CT v.f. in pure Mg single crystals. As mentioned in Section 2, CTs have been identified as a potential source of fracture initiation (Barnett, 2007; Kelley and Hosford, 1968; Wonsiewicz, 1966).

b. Higher strength in case B:
It is interesting to note that although the crystallographic orientations of A and B are similar, the stress level in case B is somewhat higher than A. We explain this as follows: in a plane-strain condition, the RSS on each system has contributions from not only the loading direction, but also from the constraint direction. With respect to the loading direction, the Schmid factor on the pyramidal $\langle c+a\rangle$ slip is 0.446 for both orientations A and B. However, the contribution from constraint direction is zero for orientation A and -0.11 for orientation B, respectively; therefore, a larger compressive stress is needed to activate the pyramidal $\langle c+a\rangle$ slip in B causing higher stress for that orientation. In addition, due to Schmid factor effect from loading and constraint direction, the prismatic slips are activated in orientation B later (Fig. 6B).

3.2.2. Compression perpendicular to the constrained c-axis (cases C and D)

As indicated in Fig. 6C and D, prismatic slip dominates the entire deformation and these predictions qualitatively agree with those of Graff et al. (2007) and Capolungo et al. (2009b). However, in contrast to these simulations, no prismatic slip

Please cite this article as: Zhang, J., Joshi, S.P., Phenomenological crystal plasticity modeling and detailed micromechanical investigations of pure magnesium. J. Mech. Phys. Solids (2012), doi:10.1016/j.jmps.2012.01.005

traces were reported in the K–H experiments (Kelley and Hosford, 1967, 1968). Wonsiewicz (1966) made identical observations as K–H, but reported that the lack of observation of the prismatic slip was likely an experimental limitation rather than its absence.

Experiments on Mg provide ample evidence that occurrence of CTs is quickly followed by fracture along CT planes (Kelley and Hosford, 1967; Reed-Hill and Robertson, 1957a, 1957b; Reed-Hill, 1960; Wonsiewicz, 1966). In other words, CTs do not contribute much to ductility, and may in fact be detrimental. Even in Mg alloys $\{10\bar{1}1\}$–$\{10\bar{1}2\}$ double twinning or $\{10\bar{1}1\}$ twinning have been reported to cause limited ductility at room temperature (Barnett, 2007). On this backdrop, the relatively large strains to failure seen in orientations C and D (Kelley and Hosford, 1967) are somewhat surprising (Fig. 5), especially that K–H reported only CT. From the current simulations (Fig. 6C and D), we posit that this observed ductility may actually be due to activation of the non-basal (prismatic) slip modes that provide stable plastic deformation through their

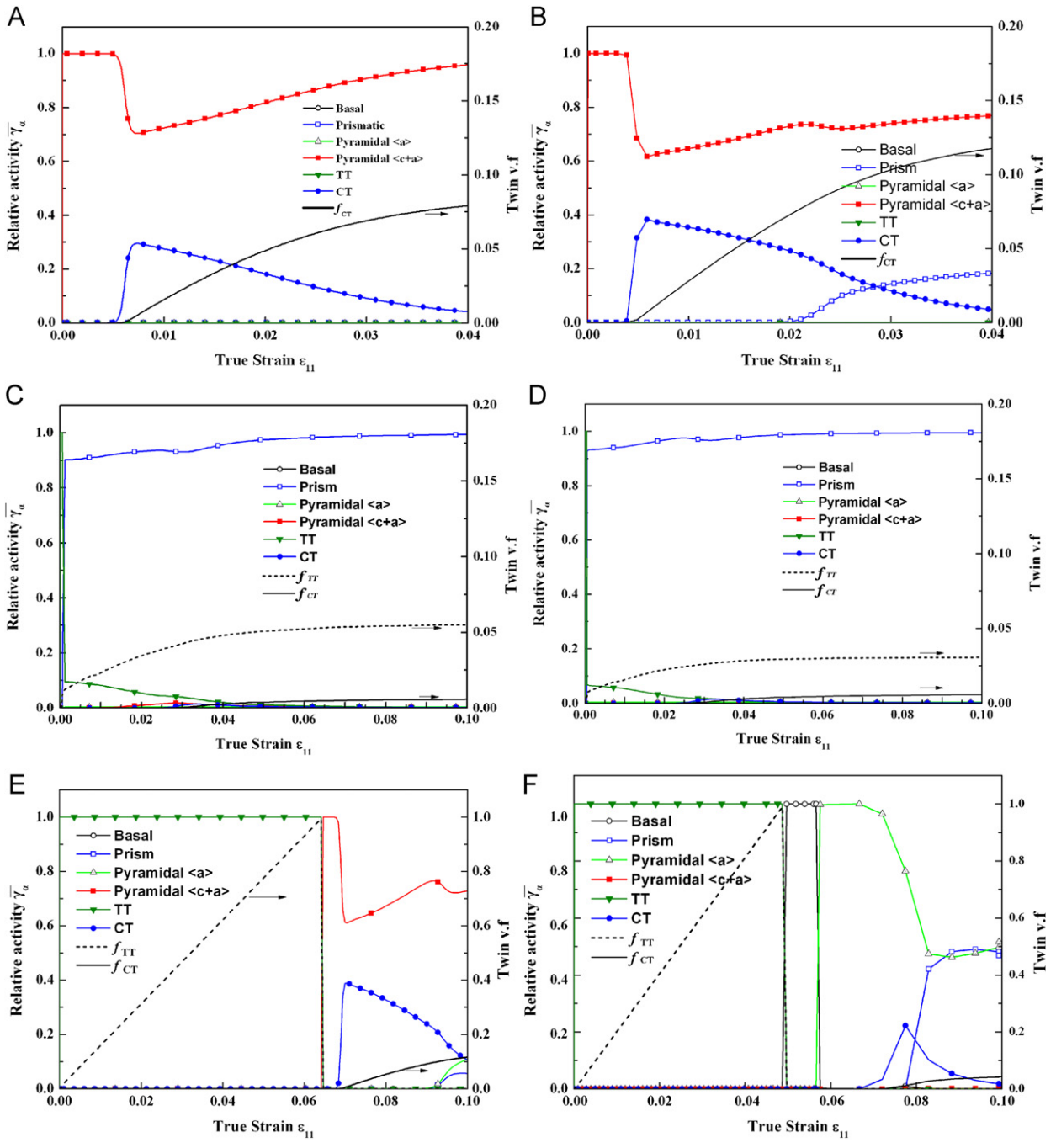

Fig. 6. (A–G) Orientation-dependent relative activities of slip and twin modes corresponding to the macroscopic responses in Fig. 5.

Please cite this article as: Zhang, J., Joshi, S.P., Phenomenological crystal plasticity modeling and detailed micromechanical investigations of pure magnesium. J. Mech. Phys. Solids (2012), doi:10.1016/j.jmps.2012.01.005

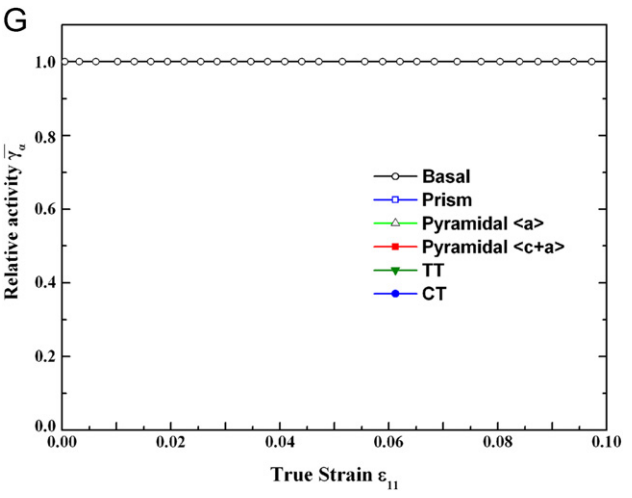

Fig. 6. (*continued*)

hardening mechanisms until the onset of CT that happens at about ~4% strain (Fig. 6C and D). Recent micro-compression experiments (Byer et al., 2010; Lilleodden, 2010) provide an interesting corroboration to this hypothesis in that only the non-basal slip activity is observed and the samples were strained up to ~10% before failure occurred.

Fig. 6C and D also show that TT is active during initial to intermediate stages of plastic deformation, albeit less dominant compared to the prismatic slip. Further, our simulations also predict small CT activity beyond ~3–4% strain in both the cases. Note that the parameters for TT have been calibrated using the initial part of orientation E (discussed et seq) and those for CT have been calibrated using orientation B, and are kept fixed here. Prima facié, the TT occurrence may appear to be at odds for these orientations given that there is a constraint along the *c*-axis (Fig. 4c and d), which resists *c*-axis extension. Although for orientations C and D the RSS from the loading direction favors TT and the RSS from the constraint direction opposes it, it turns out that the net RSS still favors TT for both C and D. It is also informative to note that the constraint plays a key role in producing much lower TT v.f. (Fig. 6C and D) compared to the scenario of unconstrained *c*-axis extension (cf. Fig. 6E and F—orientations E and F).

Although the prediction of TT and CT is consistent with the K–H experiments, the CT v.f. in both the orientations appears to be low compared to it being reported as the dominant mode observed in K–H experiments. The profuseness of CT in K–H experiments seems surprising for the C and D cases given the crystal orientations vis-à-vis the loading and constraint directions. K–H reported that some works postulate existence of two different CRSSs for the CT system, but provided no further reasoning to support it. Christian and Mahajan (1995) indicate that prior slip may play a role in the nucleation of twins in BCC metals, but it is not clear if this is also the case in HCP metals for CT. In our simulations only one CT–CRSS exists and yet, CT activity, albeit small, is predicted for these orientations. In lieu of the orientation-dependent CT–CRSS, the presence of CT in K–H experiments is rationalized here on the basis of initial TT and a slip-independent CT–CRSS. In orientations C and D, CT may be activated in several ways. One is that the Schmid factors on the CT systems result in the RSS that can activate them upon reaching the CT–CRSS. In addition, note that Fig. 6C and D predicts initial TT activity, which K–H have also reported, and as mentioned in the preceding paragraph is due to the net RSS on the TT systems being favorable for it to occur. This provides an additional likelihood of activation of the CT mode for C and D in two ways. Firstly, regions that undergo TT induced lattice reorientation pave way for subsequent occurrence of CT (akin to orientations E and F, described later). Secondly, the discreteness of TTs may provide stress concentrations that trigger some CT activity in their neighborhood. Naturally, the CT activity and v.f. is then intimately tied to the TT activity. Further, the initial TT activity and v.f. depends on the efficacy of the plane strain constraint such that if constraint walls are perfectly rigid (as in the 2D plane strain simulations) they tend to oppose TT and generate a small TT activity and v.f. This also manifests as a meager CT activity (Fig. 6C and D). On the other hand, if the walls providing the plane strain effect are elastically deformable (as mentioned in K–H experiments) they impose a *weaker* plane strain constraint that further aids initial TT leading to an enhanced CT activity and v.f. Unfortunately, these aspects cannot be revealed in a 2D plane strain simulation with pristine initial structure, and necessitates a 3D simulation together with at least a dilute amount of initial heterogeneities that can trigger non-uniform stress distribution. Therefore, as a model case, we tested this possibility by performing a 3D simulation that has a small percentage of initial regions with TT orientations randomly distributed in the matrix. Further, the weaker plane strain constraint is considered by explicitly modeling the elastically deformable channel walls (see Supplementary material, Section B). Indeed, we found that the *average* CT v.f. in these simulations almost doubled compared to the strict plane strain condition (locally, the CT v.f. may be even higher—see Fig. B-1, Supplementary material). The relative activity also gets modulated with reduced prismatic activity (Supplementary material, Fig. B-2) due to higher TT and CT activities. The slip-independent twinning assumption incorporated in the present model

Please cite this article as: Zhang, J., Joshi, S.P., Phenomenological crystal plasticity modeling and detailed micromechanical investigations of pure magnesium. J. Mech. Phys. Solids (2012), doi:10.1016/j.jmps.2012.01.005

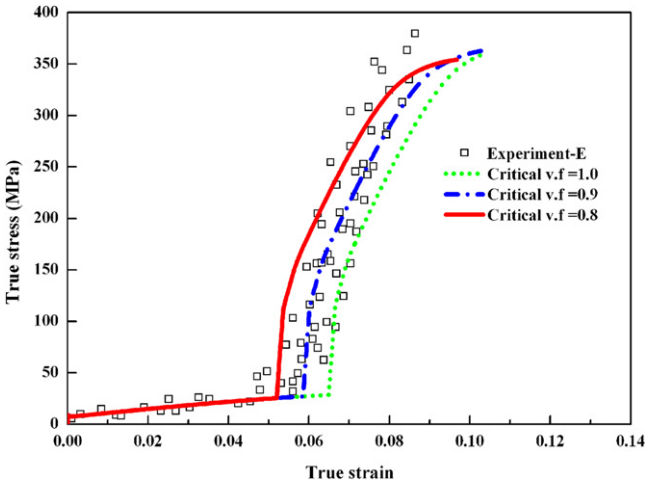

Fig. 7. Effect of critical twin volume fraction f_{cr} on the stress–strain responses (orientation E).

(Section 2.3.3) is also expected to aid the CT activity, because it liberates the prior hardening of the CT systems due to the preceding slip and TT activities and requires that only the CT–CRSS be reached for it to initiate. Although the average v.f. might still appear small, the number of compression twins can be substantial. A rough calculation with CT v.f. of ~1% assuming an average twin thickness of ~5–10 μm (Barnett, 2007) and for specimen sizes used in K–H experiments gives about 15–20 twins spaced at ~400–500 μm, which seems reasonable (Chapuis and Driver, 2010).

Finally, our separate simulations (not presented here) on *c*-axis compression of a single crystal specimen comprising a single, discrete $\{10\bar{1}1\}$ compression twin with a double twin inside, reveals high strain accumulation in the twin due to the basal slip inside them. This is consistent with K–H observations in that they also associated it with the recrystallization that occurred within the CTs. We note here that such a high strain accumulation in the narrow regions may have a tendency to cause failure, as observed in CT induced fracture in literature. A deeper understanding of the nucleation aspects of twinning, especially CTs, and the interactions between slip and DT needs further experimental evidence (Capolungo et al., 2009b; Li and Ma, 2009). Twinning in Mg continues to be an active topic of investigation (Capolungo et al., 2009b; Christian and Mahajan, 1995; Kucherov and Tadmor, 2007; Li and Ma, 2009; Meyers et al., 2001) as the governing physical mechanisms are still not fully unraveled.

3.2.3. *Compression perpendicular to the unconstrained c-axis (cases E and F)*

In case E and F, TTs dominate the deformation process before significant reorientation of the crystal lattice (Fig. 6E and F). This TT-induced reorientation then activates the CT modes and non-basal slip (i.e. pyramidal $\langle c+a \rangle$ in case E, prismatic and pyramidal $\langle a \rangle$ in case F) to accommodate further deformation and is characterized by a rapid increase in the macroscopic stress (Fig. 5, orientations E and F). As shown in Fig. 7, the macroscopic critical strain ε_c at which the rapid stress increase occurs depends on the critical twin v.f.f_{cr}(Eq. (21)) chosen for the activation of the reorientation scheme within the FE framework. It can be seen that a choice of $0.8 \leq f_{cr} \leq 1.0$ gives a reasonable macroscopic prediction, with $f_{cr}=0.9$ appearing to be a good assumption[14] :

a. Effect of initial heterogeneities:
An important distinction between the natures of the predicted and experimental curves in Fig. 5 (also Fig. 7) is the instantaneous elevation of the stress post reorientation in the former compared to a smoother transition (i.e. from a weakly hardening plateau to a strong hardening) in the latter. In the simulated pristine single crystal, this happens because the lattice is reoriented at a GP only after the twin v.f. at that point reaches f_{cr}, a condition that is satisfied in these simulations at all the GPs at the same time (corresponding to ε_c) due to a homogeneous stress state. On the other hand, real specimens possess internal heterogeneities such as lattice misorientations due to dislocation substructures, initial twin population and similar initial defects that may cause a heterogeneous stress state, and consequently, also a heterogeneous twin v.f. evolution. As a model problem to assess this effect of initial heterogeneities, we performed additional simulations with randomly chosen regions in the FE mesh that possess an initial TT orientation. The number of FEs in the bulk sample with an initial TT orientation sets up an initial TT v.f., f_0.[15] Fig. 8 shows that the macroscopic

[14] For all the simulations performed in this work, at each GP we set $f_{cr}=0.9$, unless specifically mentioned.

[15] We performed simulations with different f_0, f_{cr} and positions of initial defects within the specimen and the results indicated that the position of initial defects has a negligible effect on the macroscopic response.

Please cite this article as: Zhang, J., Joshi, S.P., Phenomenological crystal plasticity modeling and detailed micromechanical investigations of pure magnesium. J. Mech. Phys. Solids (2012), doi:10.1016/j.jmps.2012.01.005

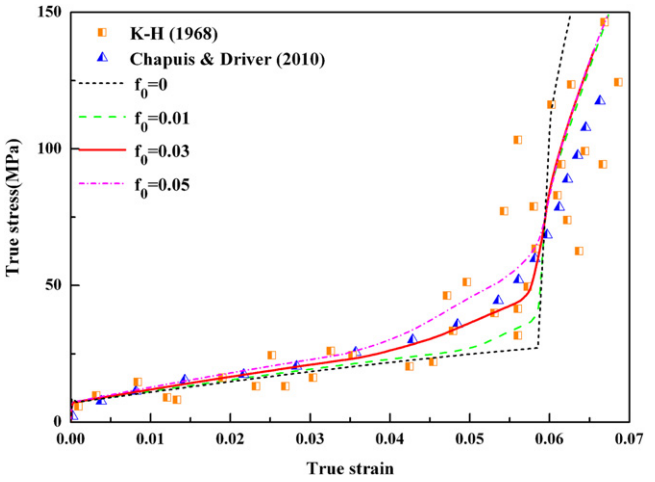

Fig. 8. Effect of the pre-existing twin population f_0 on the macroscopic stress–strain curves (f_{cr}=0.9).

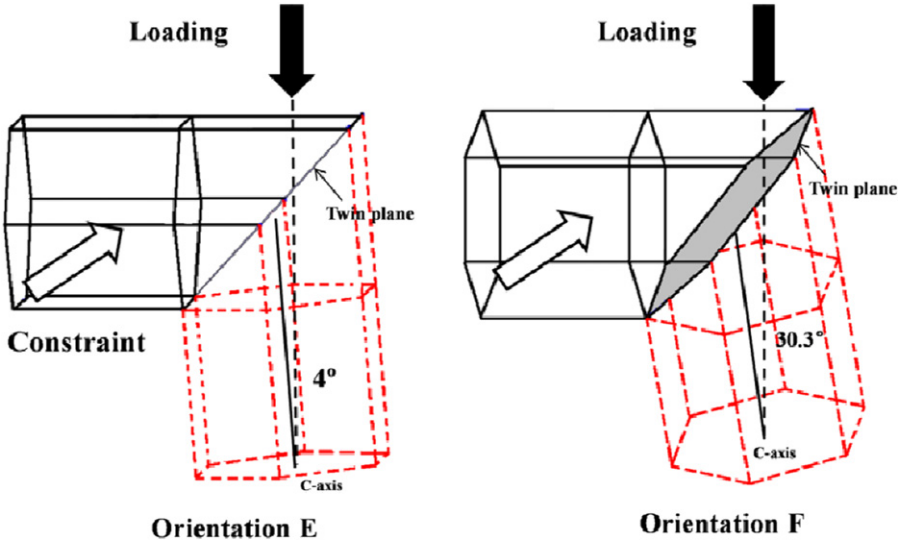

Fig. 9. Differences in the reoriented lattice configurations due to twinning in orientations E and F.

behavior with pre-existing twin population (with $0.01 \leq f_0 \leq 0.05$) mimics the K–H experiments for f_{cr}=0.9, especially for 3% initial TT v.f. Note also the good corroboration with the recent experimental results by Chapuis and Driver (2010) for the same loading condition. It is interesting to note that Clausen et al. (2008) also found improved corroboration with polycrystalline Mg alloy experiments by incorporating an initial twin v.f. of ~3% in the elasto-plastic self-consistent approach.

b. Effect of lattice-reorientation:
Although the initial orientations for cases E and F are quite similar, their macroscopic post-twinning responses are quantitatively different. Our simulations predict these differences very well without having to modify the hardening parameters and attribute it to the activation of the different twin systems based on their Schmid factors, explained as follows: of the possible six TT systems, orientation E favors two viz. the $(10\bar{1}2)[\bar{1}0\bar{1}2]$ and$(10\bar{1}2)[\bar{1}0\bar{1}1]$, one of which (based on the maximum TT v.f.) determines the eventual orientation of the lattice with the loading/constraint directions. In comparison, for orientation F one of the remaining four equally favored twinning systems reorients the lattice. Consequently, the rotated configurations due to twinning are different in the two cases. Fig. 9 shows these new lattice orientation configurations (dashed lines) with respect to the initial orientation (solid lines). Interestingly, case E that experiences ~86° reorientation of the lattice due to TT is only 4° off the original crystal orientation in the case B. This is also the reason why the post-twinning stress–strain response of case E roughly asymptotes toward that of the case B, further reinforced by the fact that the relative activities for case E (Fig. 6E) after the completion of twinning (ε_c~0.065) are remarkably similar to those observed in case B (Fig. 6B). That is, in case E the pyramidal $\langle c+a \rangle$and CT dominate the deformation after TT is complete and is only weakly augmented by the prismatic and pyramidal $\langle a \rangle$ modes. On the other hand, the twinning system activated in case F reorients the lattice such that

Please cite this article as: Zhang, J., Joshi, S.P., Phenomenological crystal plasticity modeling and detailed micromechanical investigations of pure magnesium. J. Mech. Phys. Solids (2012), doi:10.1016/j.jmps.2012.01.005

the angle between the normal to the basal plane and the loading direction is $\sim 30.3^{\circ}$, which matches closely with the experimental observation of 31° (Kelley and Hosford, 1967). This twinning-induced reorientation causes activities on the basal, prismatic and pyramidal $\langle a \rangle$ slip systems in case F that exhibit lower hardening than the pyramidal $\langle c+a \rangle$ slip and CT activated in case E. Consequently, the overall stress level reached in case F is lower than that in case E.

Graff et al. (2007) modeled the hardening for the TT friendly orientations via a power law and in the process, avoided the re-orientation scheme altogether. While that approach also fitted the K–H stress–strain responses, it concealed the possible mechanisms that could lead to such a response. Recently, El Kadiri and Oppedal (2010) proposed an interesting reasoning for a similar behavior observed in c-fiber textured Mg and Zr polycrystals. They argued that as the TTs grow (thicken) some proportion of dislocations in a parent region *transmutate* into new dislocation types on different slip systems as that region becomes a part of the twin. The resulting increased dislocation density in the twinned region arising from such a transmutation is what leads to a significant increase in the hardening when profuse twinning occurs, at least in the context of polycrystals. It is likely that this type of mechanism is also relevant in the single crystal. Although our current approach does not explicitly incorporate the transmutation mechanism, we demonstrate later that the present constitutive descriptions and their parameters capture the hardening response for *c*-fiber textured Mg polycrystal (Section 3.4) given lattice-reorientation due to TT. While such a mechanism may simply be embedded as a high initial hardening modulus in the TT–slip interaction term ($g_{tt\rightarrow sl}$), it would be useful to construct a mechanism-based constitutive description within SCP framework.

c. TT-induced sample contraction along c-axis in orientation F.

In case E, the stress in the constrained direction is always compressive. In other words, the specimen face and the channel wall are always in contact. However, in case F, the initial compressive stress during deformation (due to the plane strain constraint against Poisson extension) is replaced by loss of contact of the specimen with the walls of the die channel (i.e. loss of plane-strain condition leading to zero constraint stress) due to the activation of the four tensile twin systems. After TT is complete, the constraint direction again experiences extension, which is constrained by the die channel walls. Clearly, a 2D plane-strain simulation would not be capture this behavior as it would be unable to simulate the loss of plane-strain condition due to out-of-plane shrinking during TT and requires a 3D calculation. The out-of-plane displacement and stress–strain responses in Fig. 10 obtained from the 3D calculation, clearly capture this experimentally reported behavior (Kelley and Hosford, 1967) and the stress–strain responses for case F. The normalized contraction in Fig. 10 indicates shrinking of the specimen before completion of TT at $\sim 5\%$ strain. Following DT-induced reorientation, the sample again undergoes extension and touches the channel wall, resuming the stress contribution from the constraint direction. The small blip in the stress–strain response is reflective of the activation of basal slip for a short period, which is immediately taken over by the non-basal slip modes (Fig. 6F).

3.2.4. Basal slip (case G)

Orientation G is perfectly suited for the $(0001)\langle 11\bar{2}0 \rangle$ basal slip because the Schmid factor is the maximum, although it may activate easily in general cases too given its lowest CRSS. Fig. 6G validates this as the favored orientation for basal slip and no other mechanism is activated over the entire strain range. Experimentally, the activation of basal slip indicates good ductility but a lower overall stress.

In the following sections, we investigate the capability of the present model to predict the behaviors of single and polycrystalline pure Mg under various circumstances.

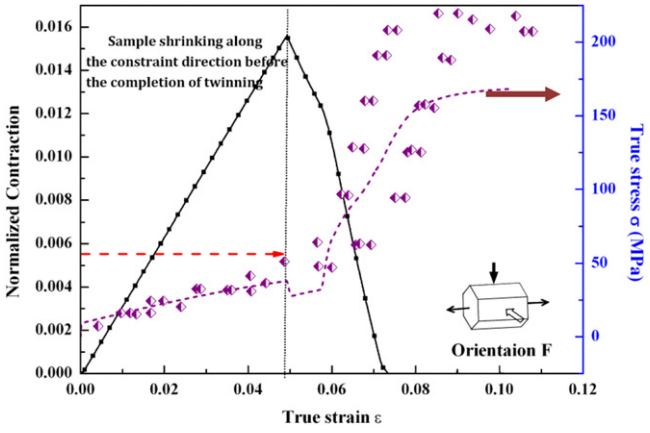

Fig. 10. Evolution of the out-of-plane deformation of specimen edge (orientation F) in initial contact with the channel wall and its corresponding stress–strain response. Increasing contraction indicates that the specimen face that was initially in contact with the channel wall is moving away from it due to the formation of tensile twins.

Please cite this article as: Zhang, J., Joshi, S.P., Phenomenological crystal plasticity modeling and detailed micromechanical investigations of pure magnesium. J. Mech. Phys. Solids (2012), doi:10.1016/j.jmps.2012.01.005

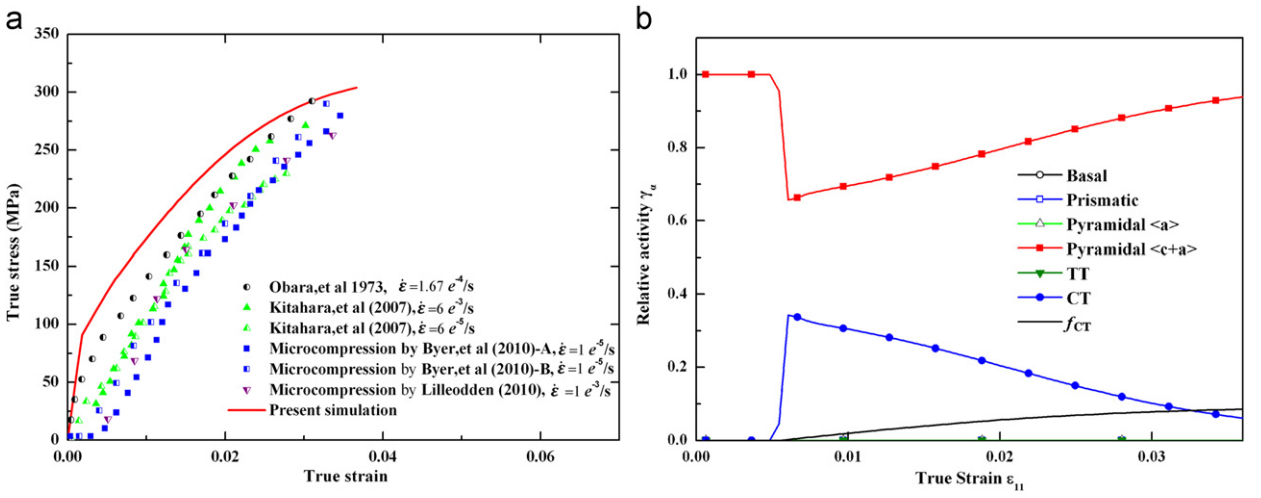

Fig. 11. Uniaxial *c*-axis compression results (a) comparison of predicted stress–strain response with experimental data and (b) predicted relative activities.

3.3. Uniaxial c-axis compression of single-crystal Mg

In the previous section, we calibrated and predicted the constitutive responses of K–H plane-strain experiments on single crystal Mg. In this section, we predict the simulation results for the uniaxial *c*-axis compression making no further modifications to the material parameters (Table 3) and compare them with experimental results. Fig. 11a shows that the predicted stress–strain response compares reasonably well with a range of experiments (Byer et al., 2010; Kitahara et al., 2007; Lilleodden, 2010; Obara et al., 1973). The relative activity plot (Fig. 11b) shows that the pyramidal $\langle c+a\rangle$ slip dominates the entire regime, but is modulated by the development of CT activity at early stages of deformation. Eventually, the pyramidal $\langle c+a\rangle$ activity picks up again as the CT v.f. development becomes sluggish. The total CT v.f. is about 0.09 at $\sim$4% global strain. As can be expected, the relative activities qualitatively resemble those corresponding to cases A and B in the preceding discussions (Fig. 8a and b). It is interesting to note that conventional the uniaxial *c*-axis compression experiments (Kitahara et al., 2007; Obara et al., 1973) report both CT and pyramidal $\langle c+a\rangle$ slip and the present results show a consistent microscopic response. In comparison, recent the uniaxial *c*-axis micro-compression experiments (Byer et al., 2010; Lilleodden, 2010) report only the pyramidal $\langle c+a\rangle$ slip over a strain range of about 10%. The question of whether specimen size promotes pyramidal $\langle c+a\rangle$ slip in lieu of CT is an interesting one, because it could help quantify the effect of CTs on the overall ductility. Although the present model does not incorporate any size-dependent mechanisms, Fig. 11b hints that the occurrence of a critical CT v.f. causing failure under c-axis compression could be inhibited or delayed if the CRSS of CT systems is more strongly size-dependent than the CRSS of the pyramidal $\langle c+a\rangle$ and/or CT systems harden more rapidly than the pyramidal $\langle c+a\rangle$ slip systems, so that the latter is always a preferred mechanism.

3.4. Polycrystal pure Mg response

In this section, we compare our predictions with the polycrystalline plane-strain experiments of Kelley and Hosford (1967) for rolled and random textures using the parameters for single crystals. In the present work, 3D polycrystalline aggregates are simulated using initial 100 single crystal orientations that are arranged as per the desired textures and each grain is meshed using a single 3D finite element (C3D8). We use the Bunge method (Randle and Engler, 2000) to determine the initial crystal orientations from the pole figure of the rolled texture (Hosford, 1993). Fig. 12a shows the initial (0001) pole figure based comprising 100 orientations that are derived from the rolled texture information in the K–H experiments. Fig. 12b shows the front face in the ZR plane for this texture. Note that the *c*-axis for individual single crystal is approximately parallel to the **Z** (**ND**) direction. Fig. 12c and d shows similar information for the random texture assumed in the present simulations. Unlike modeling of single crystals, the polycrystalline situation is complicated by the fact that individual grain misorientations and deviations from ideal (single crystal) texture become important. This directly reflects from the number of grain orientations modeled in the numerical simulation and their efficacy in representing the real texture. The limited number of grains and their orientations is expected to affect the result. Our primary goal here is to show that the constitutive model developed and the parameters obtained for single crystals capture the trend adequately. The quantitative deviations may be ascribed to the limited information on the grain orientations and deviations from the real textures. Additional mechanisms emanating from grain boundaries (gb's), such as gb sliding (Staroselsky and Anand, 2003), hardening of plastic slip by accumulated dislocations at gb's, and gb mediated probabilistic twinning nucleation

Please cite this article as: Zhang, J., Joshi, S.P., Phenomenological crystal plasticity modeling and detailed micromechanical investigations of pure magnesium. J. Mech. Phys. Solids (2012), doi:10.1016/j.jmps.2012.01.005

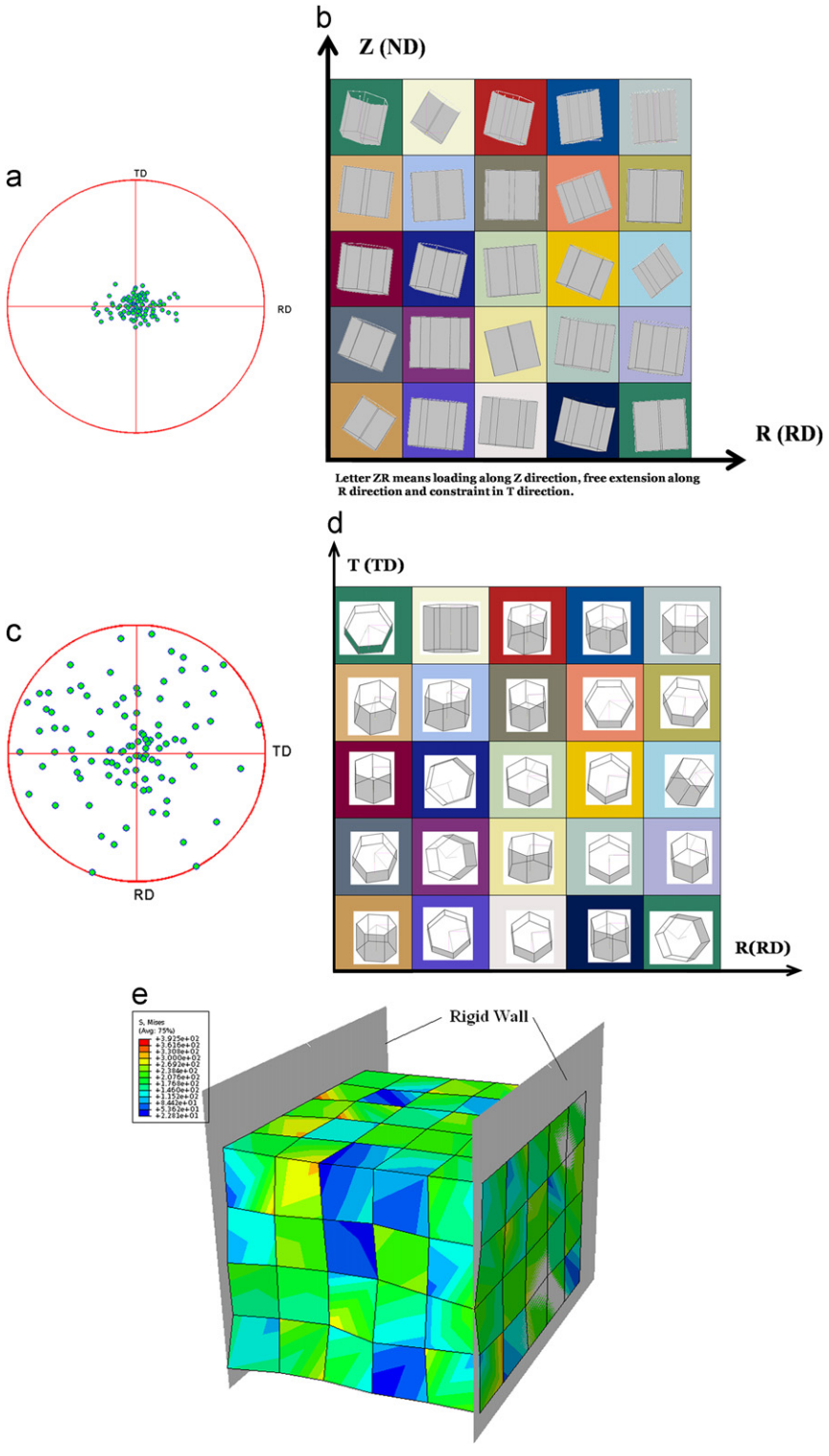

Fig. 12. (a) Simulated (0001) pole figure for polycrystalline pure Mg with a rolled texture, (b) corresponding grain orientations in the frontal ZR plane, (c) simulated (0001) pole figure for a polycrystalline pure Mg with random texture, (d) corresponding grain orientations in the frontal RT plane, and (e) heterogeneous von Mises stress distribution in the random textured polycrystal Mg.

Please cite this article as: Zhang, J., Joshi, S.P., Phenomenological crystal plasticity modeling and detailed micromechanical investigations of pure magnesium. J. Mech. Phys. Solids (2012), doi:10.1016/j.jmps.2012.01.005

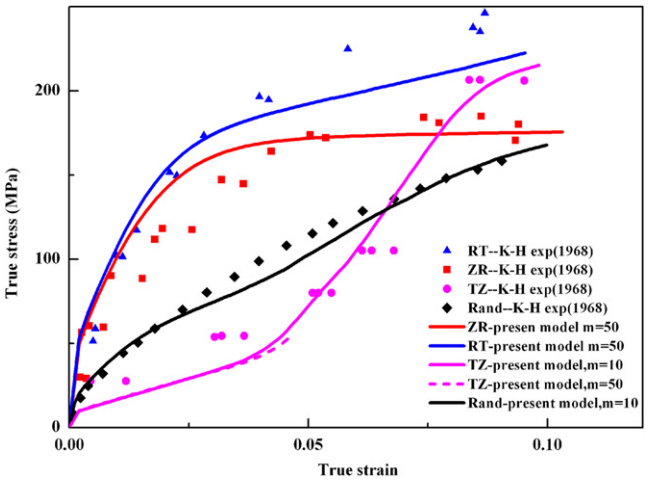

Fig. 13. Comparison of plane-strain compression experiments (symbols) on polycrystalline pure Mg with predicted results (lines).

(Beyerlein et al., 2010, 2011) are not incorporated in the current framework. We compare our predictions with the polycrystalline plane-strain experiments of Kelley and Hosford (1967) comprising rolled and random textures.

Fig. 13 compares the simulated macroscopic stress–strain responses for the textured and random polycrystal models with the experimental data. Even with the limited number of initial grain orientations and coarse FE meshes, the general trends are well reproduced for all the curves. It is also seen that the trends of the predicted hardening rate curves for polycrystalline Mg compare reasonably with the experiments (Supplementary material, Fig. A-2). Fig. 14a–d provides the corresponding evolution of the volume-averaged relative slip and twin activities as defined in Eq. (29). The averaged twin v.f., $\overline{f}_{CT}$ and $\overline{f}_{TT}$ are defined as the volume average of twin v.f. at all material points for CT and TT modes, respectively. For hcp aggregate, inter-granular interactions are important owing to the low crystallographic symmetry and higher anisotropic plastic behaviors of the individual grains. Unlike viscoplastic self-consistent models that calculate homogenized intra- and inter-granular stresses, in the present modeling approach the stress concentrations and gradients can be explicitly obtained (Fig. 12e) and can be further resolved with finer FE meshes (Choi et al., 2010).

The *ZR* texture deviates from the ideal single crystal orientations A and B (Fig. 6A and B) by the small misalignments of the individual grains in the polycrystalline specimen (Fig. 12b). As shown in Fig. 14a, this triggers pyramidal $\langle a \rangle$ and basal slip activities, which tempers down the relative importance of the pyramidal $\langle c+a \rangle$ and CT and causes the macroscopic stress level to be somewhat smaller compared to its ideal single crystal counterparts (Fig. 7). Note that Nave and Barnett (2004) clearly show the occurrence of CT, but these have not been reported or modeled by most crystal plasticity modeling approaches of the similar kind.

The *TZ* response (Fig. 13) bears resemblance with orientation E (Fig. 5), because the latter can be considered as the special case of the former if all the grains within the polycrystal were to be perfectly aligned with the thickness direction of the specimen. The relative activity is dominated by the $\{10\bar{1}2\}$ TT mode (Fig. 14c) up to about 4% macroscopic strain and the small deviations from the ideal *c*-axis orientations trigger the basal slip activity. The TT v.f. evolution is not shown in this figure and is discussed separately (Fig. 14e—*TZ*). It should be noted here that with $m=50$ the numerical cost for the TZ orientation (blue dashed line) is huge as convergence becomes increasingly difficult and time-consuming closer to the saturation of TT evolution and activation of DT-induced lattice reorientation in most grains.[16] Keeping all the other parameters the same but modifying m to be equal to 10, the predicted response (blue solid line) curve is identical to the one with $m=50$, but importantly, the convergence rate is vastly improved leading to an extended comparison over a much larger strain range. Fig. 14c also shows the pyramidal slip and CT activity that initiates inside the twinned v.f. post reorientation. Note that unlike its single crystal degenerates (orientations E and F, Fig. 6E and F) here the TT-induced lattice reorientation is a cascading process, because each crystal evolves differently. In order to quantify the process of TT-induced reorientation, we define a ratio $\overline{n}$ in the FE context as

$$\overline{n} = K_{GP}^{tw}/N_{GP} \tag{31}$$

where K_{GP}^{tw} is the number of GPs where the lattice is reoriented due to the TT and N_{GP} is the total number of GPs in the polycrystalline sample. It is only at around a macroscopic strain of $\sim$9% that almost all grain area undergoes the reorientation process (Fig. 14e—TZ). Concomitantly, beyond $\sim$6% strain the pyramidal $\langle a \rangle$ slip begins to take over as a dominant mode thanks to the already reoriented crystals and is augmented by CT (Fig. 14c). Fig. 14c also shows that the slip systems in TT regions are activated (dashed orange curve) while the overall twinning is still active. This is because as

[16] We ran several attempts by changing the mesh size, but it took on an average about 3000 CPU hours to reach a strain of $\sim$5% with $m=50$.

Please cite this article as: Zhang, J., Joshi, S.P., Phenomenological crystal plasticity modeling and detailed micromechanical investigations of pure magnesium. J. Mech. Phys. Solids (2012), doi:10.1016/j.jmps.2012.01.005

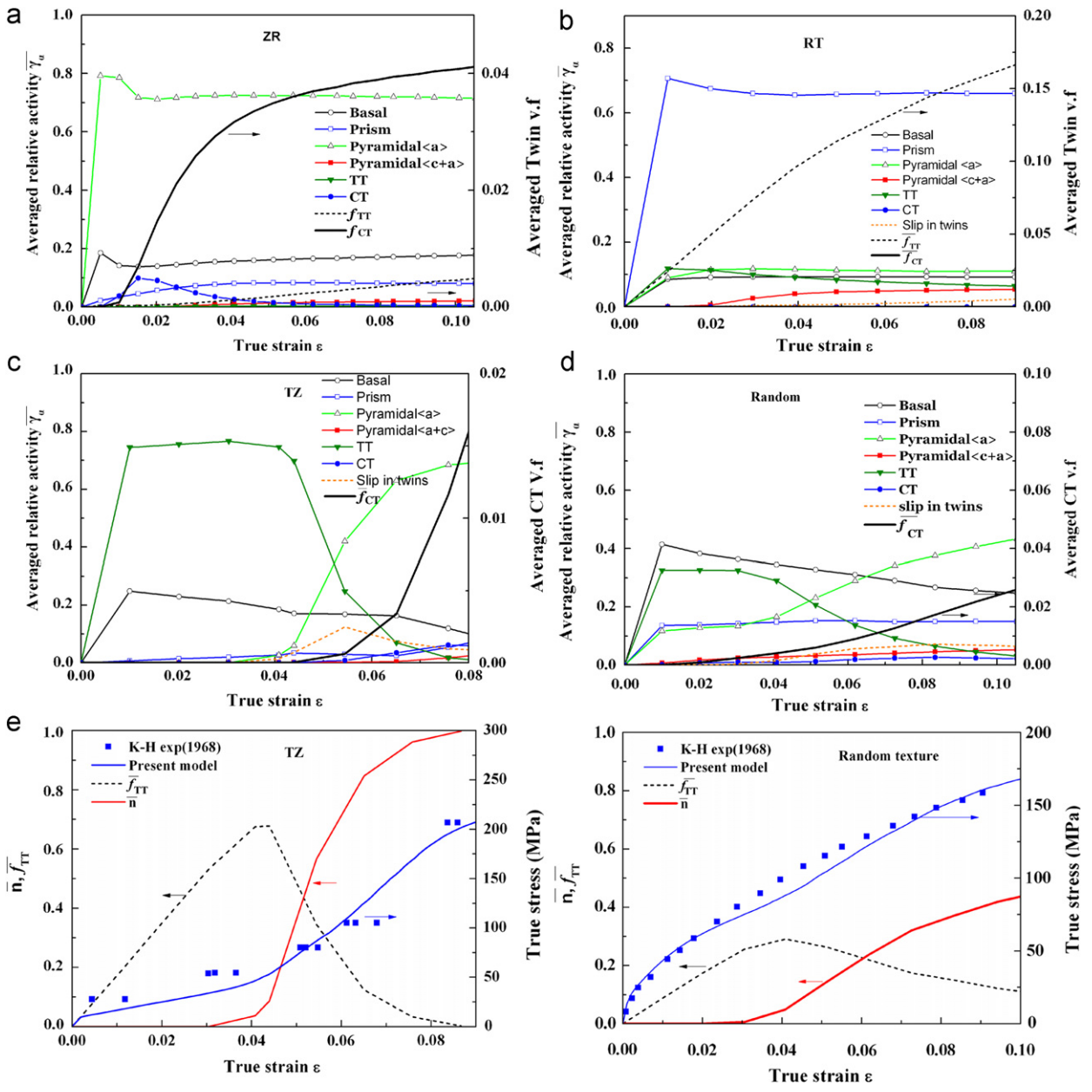

Fig. 14. Relative activities in textured polycrystal Mg: (a) ZR case, (b) RT case, (c) TZ case, and (d) random texture. Evolution of (e) average TT v.f. $\overline{f}_{TT}$ and TT-induced reoriented fraction of GPs $\overline{n}$ in TZ and random textures. For interpretation of the references to color in this figure, the reader is referred to the web version of this article.

TT v.f. at every GP evolves heterogeneously the third term on the right-hand side of Eq. (2) activates. The contribution to this slip activity within the twinned regions must mostly come from the basal slip mode thanks to its lowest CRSS and the non-ideal orientations of individual grains (unlike cases E and F). In the single crystal degenerate cases (orientation E) too, the slip in twinned regions is theoretically possible only for non-basal modes (because basal planes are almost normal to the loading direction), but are not activated due to their high CRSS and hardening that follows due to the contribution from the plastic strain from TT. Interestingly, in comparison to the *TZ* case, there is also small slip activity observed in the twinned regions for *RT* case (Fig. 14a and b), but not in the *ZR*. Although, some activity must be present in *ZR* case too, it is tempered by the low TT v.f. compared to its *TZ* counterpart (Eq. (2)) and they are negligibly small to show up in the relative activities' plot.

The macroscopic response of the randomly textured polycrystal is intermediate to those of its textured counterparts (Fig. 13), and is modulated by the two easiest modes—the basal slip and TT (Fig. 14d). This confirms the experimental

Please cite this article as: Zhang, J., Joshi, S.P., Phenomenological crystal plasticity modeling and detailed micromechanical investigations of pure magnesium. J. Mech. Phys. Solids (2012), doi:10.1016/j.jmps.2012.01.005

indication that basal slip remains the primary deformation mode Mg in random polycrystals (Hauser et al., 1955). The non-basal slip modes and CT show negligible presence in the initial stages and become discernible only at the later stages of the deformation. Further, like in the *TZ* case the slip in the region reoriented by TT is active over most of the deformation beyond about 3% strain (orange dashed curve), given the sizable TT v.f. (Fig. 14e—random). However, only about 40% of the total number of GPs are reoriented due to TT at about 10% macroscopic strain.

Given that only 100 grain orientations are modeled and the FE mesh discretization is coarse (1 element per grain), the predictions in Figs. 13 and 14 appear to compare reasonably well with experiments. With improved sampling from the grain orientation distribution space together with fine FE meshes the results are expected to be better.

3.5. Crystal plasticity of Mg composites

With the encouraging corroborations in the preceding sections between our computational simulations and a wide range of experiments for single and polycrystalline pure Mg, we now report preliminary investigations of the orientation-dependent characteristics of a pure Mg crystal in the presence of stiff, elastic inclusions. The motivation comes from the necessity to interpret the macroscopic responses in terms of the evolution of local deformation characteristics mediated by stiff inclusions, as a first step toward understanding the mechanics of strong Mg composite architectures, mentioned in the Introduction section. It can be imagined that several parameters including Mg texture, grain size, inclusion size, v.f., shape and orientation would mediate the deformation characteristics and the overall response of Mg composites. While such an exposition would be quite involved, we may start with a significantly simpler setting while alluding to these complexities. With this in mind, we consider an Mg single crystal with embedded elastic inclusion (Fig. 15), deformed under *c*-axis tension or compression. Although it would be ideal to investigate a wide range of orientations as in Section 3.2, we choose these two cases primarily because they activate some of the softest (e.g. TT) and hardest (non-basal modes) deformation systems. Secondly, they provide limiting cases for textured polycrystals (e.g. *ZR* and *TZ* orientations).

Symmetric displacement boundary conditions are applied to the left and bottom edges of the microstructure and the right edge is allowed to translate horizontally, but constrained to remain straight during the deformation. These conditions roughly mimic a bulk material with grains that are much bigger than the inclusions. The inclusion v.f. $f_i=0.10$ and its Young's modulus and Poisson's ratio as 375 GPa and 0.22, respectively. The interface is assumed to be perfectly bonded and the unit cell is finely meshed with 2D plane strain FEs (CPE3).

Fig. 16 shows the true stress–true strain responses for the composite loaded along the *c*-axis. While the *c*-axis compressive response improves only marginally, the corresponding tensile response is modified significantly.

Although not shown here for brevity, for the compressive response the pyramidal $\langle c+a \rangle$ slip remains the dominant mode irrespective of whether an inclusion is present or not. Further, the maximum average CT v.f. is nearly the same as its monolithic counterpart, but the distribution is more inhomogeneous in the former.

Under c-axis tension, the monolithic Mg single crystal shows a homogeneous stress state and as reported earlier (Figs. 5 and 7), the entire grain reorients due to TT at $\varepsilon_c \sim 0.06$ strain. For the corresponding composite architecture, the hardening is more gradual. It is interesting to compare the trend in Fig. 16 with that in Fig. 8 where the inclusions (initial twins) are elasto-plastically softer. The hardening of the tensile response in the presence of stiff, elastic inclusions (Fig. 16) is significantly stronger than that achieved with an elasto-plastically deforming inclusion (Fig. 8). This is a result of the strength of TT-induced texture evolution, which is relatively weak for a softer inclusion compared to a harder inclusion, at a given strain.

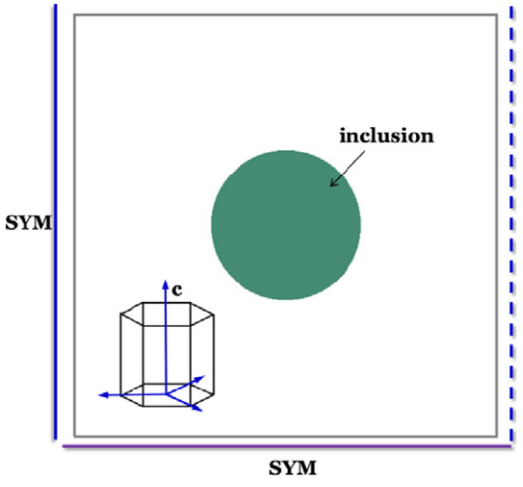

Fig. 15. Crystal orientation and boundary conditions used in unit cell Mg-composite simulations.

Please cite this article as: Zhang, J., Joshi, S.P., Phenomenological crystal plasticity modeling and detailed micromechanical investigations of pure magnesium. J. Mech. Phys. Solids (2012), doi:10.1016/j.jmps.2012.01.005

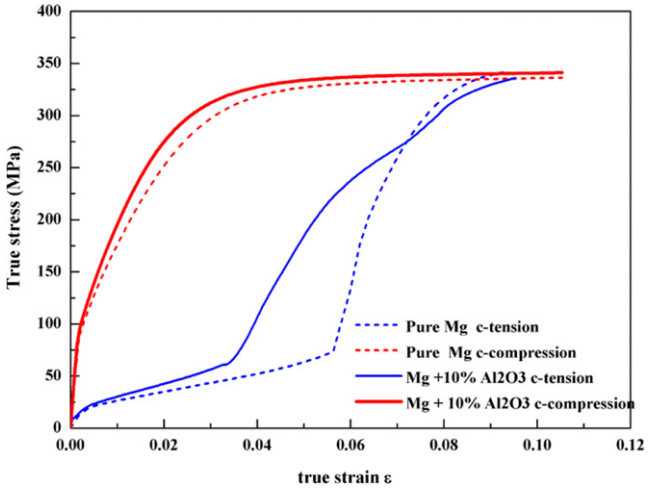

Fig. 16. Orientation-dependent true stress–true strain responses for monolithic and composite Mg.

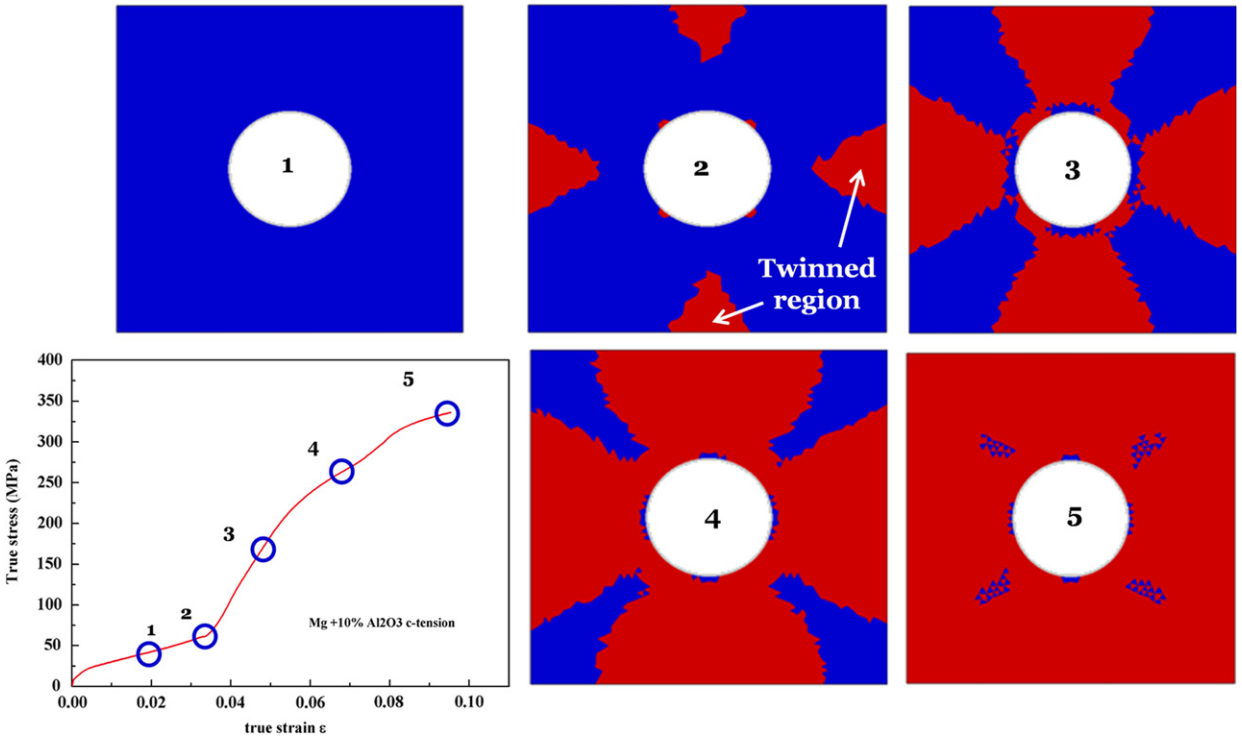

Fig. 17. Evolution of TT in Mg composite unit cell under *c*-axis tension. For interpretation of the references to color in this figure, the reader is referred to the web version of this article.

As shown in Fig. 17 the TT evolution is inhomogeneous in the presence of the stiff inclusion. In this figure, regions reoriented (i.e. satisfying the local condition $f_{tt}=f_{cr}$) due to TT are shown in red whereas those that yet to reorient are shown in blue. Interestingly, the TT distribution is more profuse away from the inclusion indicating that an inclusion provides a strong constraint to this mode of deformation in its vicinity. Although this twinning begins to emerge at much lower strain ($\sim$0.035) compared to the monolithic Mg single crystal, only at $\varepsilon_c\sim$0.10 does the entire matrix region twin. In other words, although the TT induced matrix reorientation may commence earlier in the presence of an inclusion it reaches a fully twinned state at a much later stage compared to the monolithic Mg owing to the strong constraint provided by the inclusion in its vicinity (Stanford and Barnett, 2009). During this evolutionary period (i.e. $\varepsilon=0.035$–0.1) the composite also exhibits enhanced hardening compared to the monolithic Mg and can be explained using Fig. 18. As seen in this figure, TT dominates the overall plasticity initially, albeit in a heterogeneous manner, and the fully reoriented regions

Please cite this article as: Zhang, J., Joshi, S.P., Phenomenological crystal plasticity modeling and detailed micromechanical investigations of pure magnesium. J. Mech. Phys. Solids (2012), doi:10.1016/j.jmps.2012.01.005

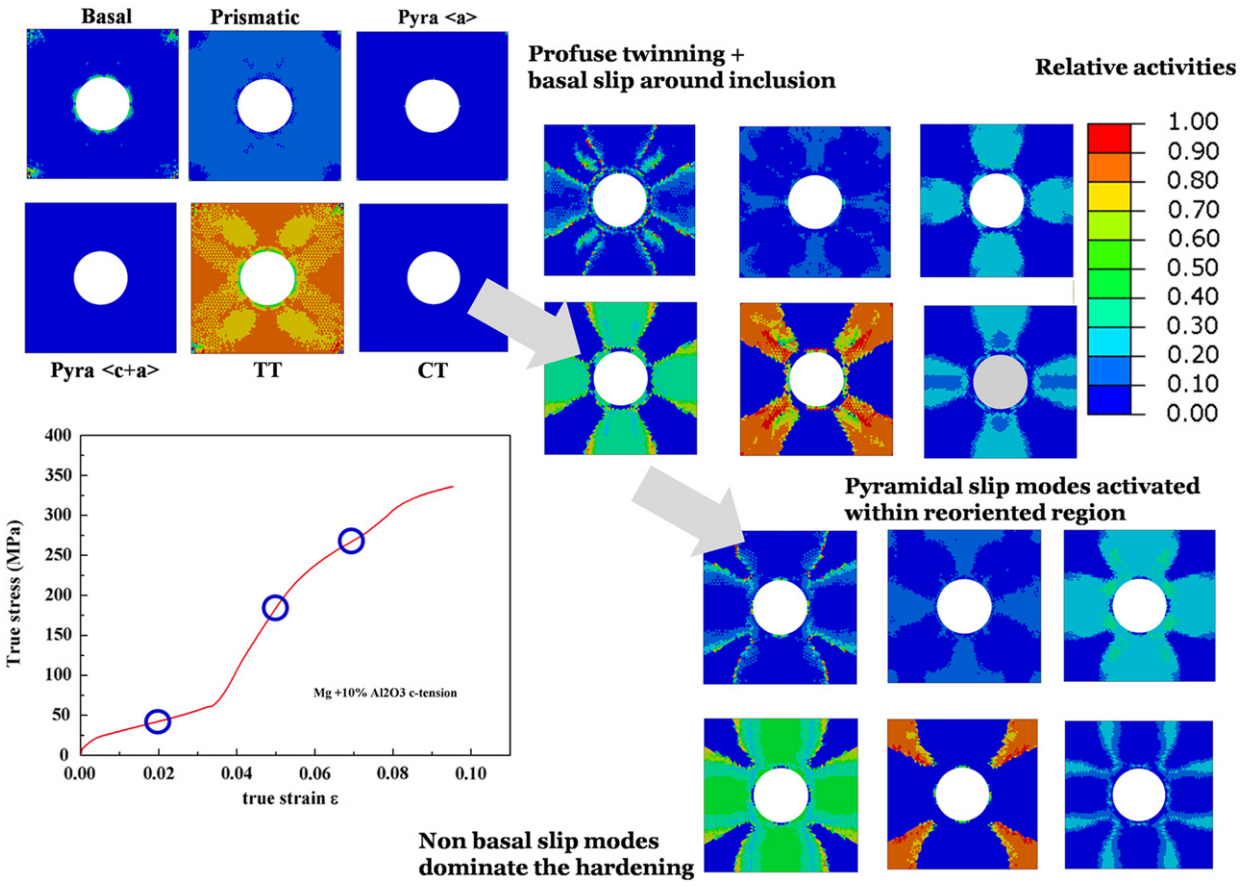

Fig. 18. Evolution of slip and twinning in the composite unit cell under *c*-axis tension.

begin to deform plastically via non-basal slip. It is this early activation of the hard non-basal modes that results in the enhanced composite hardening. Gupta and co-workers (e.g. Habibi et al., 2010; Zhong et al., 2007) have consistently reported signatures of non-basal slip activated in the uniaxial compression of extruded pure Mg polycrystalline matrices in the presence of various types of reinforcements. Fig. 18 qualitatively and quantitatively cascades the evolving interaction between the TT and different slip modes. Note that with inclusions, the overall response approaches the compressive response and tends to reduce the strength anisotropy that is otherwise commonly observed in Mg. An interesting aspect that arises from this result is whether one can devise microstructures that can minimize the anisotropy in Mg polycrystals. It appears that a judicious use of reinforcement sizes, shapes, mechanical properties of inclusion and v.f.'s may be a useful strategy in achieving this goal (Habibi et al., 2010; Robson et al., 2011). There may also be other possibilities, e.g. grain refinement that can be adopted concurrently in order to mitigate the texture induced yield anisotropy in Mg (Li et al., in press) together with strengthening. Further detailed investigations on such global–local correspondences can shed light on designing novel Mg composite architectures that are strong and ductile (Habibi et al., 2010; Zhong et al., 2007).

4. Conclusions

In this work, we have presented an SCP model for pure Mg single crystals incorporating hardening laws for key slip and twin modes and expressing their interactions that are derived from experimental evidences. While these hardening laws are still phenomenological and may not fully describe the myriad interactions between different mechanisms, they are based on physical arguments especially for the twin–twin, twin–slip and slip–twin interactions in pure Mg. In doing so, we have attempted to retain the conventional structure of the self and latent hardening adopted in most SCP frameworks. The model emphasizes the differences between tension and compression twin evolution characteristics in Mg and their role in the slip and twin hardening, because they are deemed important in the overall response including strengthening and ductility. Using these modified laws, the computational results have been critically evaluated and they compare well, both macroscopically and microscopically, vis-à-vis a wide range of experimental results including uniaxial and plane-strain compression of single crystals and plane-strain polycrystals with different textures. The dilemma about the orientation-dependent occurrence of CT in single crystal c-axis plane-strain compression experiments is partly attributed

Please cite this article as: Zhang, J., Joshi, S.P., Phenomenological crystal plasticity modeling and detailed micromechanical investigations of pure magnesium. J. Mech. Phys. Solids (2012), doi:10.1016/j.jmps.2012.01.005

to the postulate that the strength of the compression twinning systems could be independent of the preceding slip evolution so that twinning may activate so long as its CRSS is reached. This is especially important for CT because their occurrence may have adverse implications on the overall ductility and therefore, they need to be appropriately accounted for. Also, it should be noted that the severity of the constraint for plane-strain compression will show some influence on relative activation of slip and twin modes.

The presence of heterogeneities such as initial misorientations or elastic inclusions mediates the local deformation mechanisms in its neighborhood, but their manifestation in the average stress–strain response may vary depending upon the inclusion stiffness and matrix crystal orientation. For the TT friendly single crystal orientations under a nominally homogeneous loading, the smooth rather than instantaneous hardening transition concomitant with the DT-induced lattice reorientation may be effected by an initial defect population that may prevail as initial twins, cell-walls, misorientations, and so forth. Extending this further, a TT friendly crystal orientation exhibits a significantly hardened response in the presence of a stiff, elastic circular inclusion compared to identically oriented monolithic Mg crystal. In comparison, the compressive loading along the c-axis shows a meager influence from the same inclusion type and v.f. The limited scenarios considered here create exciting avenues to perform detailed SCP investigations on the roles that inclusion stiffness, shape, v.f. and orientation would play in the local characteristics of Mg crystals in an attempt to enhance their strength and tune their anisotropic macroscopic behavior (Habibi et al., 2010). These simulations could also serve as an initial step toward incorporating length-scale effects in the Mg SCP framework that would enable probing the effects of inclusion size on the overall response (Robson et al., 2011). Our ongoing work in this direction is focused on modeling the orientation-dependent responses of single and polycrystalline pure Mg in the presence of different types of discrete defects including twins, elasto-plastic second-phase inclusions, voids and cracks.

The bottom–up approach from single to polycrystalline simulations provides several exciting prospects. It provides a way to explicitly investigate effects of grain orientation, size and shape distribution effects. The approach could be further enhanced by accounting for grain boundary effects such as grain boundary sliding (Staroselsky and Anand, 2003), probabilistic descriptions of the twin nucleation (Beyerlein et al., 2010; Beyerlein and Tomé, 2010). One possible way to model the grain boundary effects is to write special constitutive laws for grain boundaries as a function of GB misorientation. Another important direction would be systematically incorporating the effects of alloying elements on the slip and twin system characteristics of single crystals (Kelley and Hosford, 1967; Akhtar and Teghtsoonian, 1969a, 1969b). Also, the temperature dependence of the slip and twin modes of single crystals would be a vital extension (Chapuis and Driver, 2010) to render its utility in addressing formability and texture evolution.

Acknowledgments

The authors acknowledge financial support from NUS-AcRF Tier 2 Grant no. R-265-000-294-133, US Army's International Technology Center-Pacific (ITC-PAC, Program Manager: Dr. J.P. Singh) through research contract nos. FA5209-10-P-0047 (R-265-000-338-597), and NSF-SERC Materials World Network Program Grant no. R-265-000-373-305.

Appendix A. Supplementary information

Supplementary data associated with this article can be found in the online version at doi:10.1016/j.jmps.2012.01.005.

References

Agnew, S.R., Brown, D.W., Tomé, C.N., 2006. Validating a polycrystal model for the elastoplastic response of magnesium alloy AZ31 using in situ neutron diffraction. Acta Mater. 54 (18), 4841–4852.

Agnew, S.R., Yoo, M.H., Tomé, C.N., 2001. Application of texture simulation to understanding mechanical behavior of Mg and solid solution alloys containing Li or Y. Acta Mater. 49 (20), 4277–4289.

Akhtar, A., Teghtsoonian, E., 1969a. Solid solution strengthening of magnesium single crystals—I alloying behaviour in basal slip. Acta Metall. 17 (11), 1339–1349.

Akhtar, A., Teghtsoonian, E., 1969b. Solid solution strengthening of magnesium single crystals—II. Tthe effect of solute on the ease of prismatic slip. Acta Metall. 17 (11), 1351–1356.

Al-Samman, T., Li, X., Chowdhury, S.G., 2010. Orientation dependent slip and twinning during compression and tension of strongly textured magnesium AZ31 alloy. Mater. Sci. Eng. A 527 (15), 3450–3463.

Ando, S., Harada, N., Tsushida, M., Kitahara, H., Tonda, H., 2007. Temperature dependence of deformation behavior in magnesium and magnesium alloy single crystals. Key Eng. Mater. 345, 101–104.

Ando, S., Ikejiri, Y., Iida, N., Tsushida, M., Tonda, H., 2006. Orientation dependence of fatigue crack propagation in magnesium single crystals. J. Jpn. Inst. Met. 70 (8), 634–637.

Aydiner, C.C., Bernier, J.V., Clausen, B., Lienert, U., Tomé, C.N., Brown, D.W., 2009. Evolution of stress in individual grains and twins in a magnesium alloy aggregate. Phys. Rev. B 80 (2) 024113 (1–6).

Barnett, M.R., 2007. Twinning and the ductility of magnesium alloys, Part II."Contraction" twins. Mater. Sci. Eng. A 464 (1–2), 8–16.

Barnett, M.R., Keshavarz, Z., Beer, A.G., Ma, X., 2008. Non-Schmid behaviour during secondary twinning in a polycrystalline magnesium alloy. Acta Mater. 56 (1), 5–15.

Please cite this article as: Zhang, J., Joshi, S.P., Phenomenological crystal plasticity modeling and detailed micromechanical investigations of pure magnesium. J. Mech. Phys. Solids (2012), doi:10.1016/j.jmps.2012.01.005

Beyerlein, I.J., Capolungo, L., Marshall, P.E., McCabe, R.J., Tomé, C.N., 2010. Statistical analyses of deformation twinning in magnesium. Philos. Mag. 90 (16), 2161–2190.
Beyerlein, I.J., McCabe, R.J., Tomé, C.N., 2011. Effect of microstructure on the nucleation of deformation twins in polycrystalline high-purity magnesium: a multi-scale modeling study. J. Mech. Phys. Solids 59 (5), 988–1003.
Beyerlein, I.J., Tomé, C.N., 2010. A probabilistic twin nucleation model for HCP polycrystalline metals. Proc. R. Soc. A 466 (2121), 2517–2544.
Boiko, V.S., Garber, R.I.G., Kosevich, A.M., 1994. Reversible Crystal Plasticity. Springer.
Brown, D.W., Agnew, S.R., Bourke, M.A.M., Holden, T.M., Vogel, S.C., Tomé, C.N., 2005. Internal strain and texture evolution during deformation twinning in magnesium. Mater. Sci. Eng. A 399 (1–2), 1–12.
Burke, E.C., Hibbard, W.R., 1952. Plastic deformation of magnesium single crystals. Trans. Metall. Soc. AIME 194, 295–303.
Byer, C.M., Li, B., Cao, B., Ramesh, K.T., 2010. Microcompression experiments on single crystal magnesium. Scr. Mater. 62, 536–539.
Caceres, C.H., Lukac, P., 2008. Strain hardening behaviour and the Taylor factor of pure magnesium. Philos. Mag. 88 (7), 977–989.
Cahn, R.W., 1953. Plastic deformation of alpha-uranium; twinning and slip. Acta Metall. 1 (1), 49–52 IN41–IN45, 53–70.
Capolungo, L., Beyerlein, I.J., Kaschner, G.C., Tomé, C.N., 2009a. On the interaction between slip dislocations and twins in HCP Zr. Mater. Sci. Eng. A 513–514, 42–51.
Capolungo, L., Beyerlein, I.J., Tomé, C.N., 2009b. Slip-assisted twin growth in hexagonal close-packed metals. Scr. Mater. 60 (1), 32–35.
Chapuis, A., Driver, J., 2010. Temperature dependency of slip and twinning in plane strain compressed magnesium single crystals. Acta Mater. 59 (5), 1986–1994.
Choi, S.–H., Kim, D.H., Park, S.S., You, B.S., 2010. Simulation of stress concentration in Mg alloys using crystal plasticity finite element method. Acta Mater. 58, 320–329.
Christian, J.W., Mahajan, S., 1995. Deformation twinning. Prog. Mater. Sci. 39 (1–2), 1–157.
Clausen, B., Tomé, C.N., Brown, D.W., Agnew, S.R., 2008. Reorientation and stress relaxation due to twinning: modeling and experimental characterization for Mg. Acta Mater. 56 (11), 2456–2468.
Couret, A., Caillard, D., 1985a. An in situ study of prismatic glide in magnesium—I. The rate controlling mechanism. Acta Metall. 33 (8), 1447–1454.
Couret, A., Caillard, D., 1985b. An in situ study of prismatic glide in magnesium—II. Microscopic activation parameters. Acta Metall. 33 (8), 1455–1462.
Crocker, A., 1962. Double twinning. Philos. Mag. 7, 1901–1924.
El Kadiri, H., Oppedal, A.L., 2010. A crystal plasticity theory for latent hardening by glide twinning through dislocation transmutation and twin accommodation effects. J. Mech. Phys. Solids 58 (4), 613–624.
Gharghouri, M.A., Weatherly, G.C., Embury, J.D., 1998. The interaction of twins and precipitates in a Mg—7.7 at% Al alloy. Philos. Mag. A 78 (5), 1137–1149.
Graff, S., Brocks, W., Steglich, D., 2007. Yielding of magnesium: from single crystal to polycrystalline aggregates. Int. J. Plast. 23 (12), 1957–1978.
Groh, S., Marin, E.B., Horstemeyer, M.F., Bammann, D.J., 2009. Dislocation motion in magnesium: a study by molecular statics and molecular dynamics. Model. Simul. Mater. Sci. Eng. 17 (7), 1–15 075009.
Habibi, M.K., Joshi, S.P., Gupta, M., 2010. Hierarchical magnesium nano-composites for enhanced mechanical response. Acta Mater. 58 (18), 6104–6114.
Hartt, W.H., Reed-Hill, R.E., 1968. Internal deformation and fracture of second-order {1011}–{1012} twins in magnesium. Trans. Metall. Soc. AIME 242, 1127–1133.
Hauser, F., Starr, C., Tietz, L., Dorn, J., 1955. Deformation mechanisms in polycrystalline aggregates of magnesium. Trans. Am. Soc. Met. 47, 102–134.
Hirsch, P., Lally, J., 1965. The deformation of magnesium single crystals. Philos. Mag. 12 (117), 595–648.
Hosford, W.F., 1993. The Mechanics of Crystals and Textured Polycrystals. Oxford University Press, New York.
Izadbakhsh, A., Inal, K., Mishra, R.K., Niewczas, M., 2011. New crystal plasticity constitutive model for large deformation in single crystals of magnesium. Comput. Mater. Sci. 50, 2185–2202.
Kalidindi, S.R., 1998. Incorporation of deformation twinning in crystal plasticity models. J. Mech. Phys. Solids 46 (2), 267–271.
Kalidindi, S.R., 2001. Modeling anisotropic strain hardening and deformation textures in low stacking fault energy fcc metals. Int. J. Plast. 17 (6), 837–860.
Kelley, E.W., Hosford, W.F., 1968. Plane-strain compression of magnesium and magnesium alloy crystals. Trans. Met. Soc. AIME 242 (1), 5–13.
Kelley, E.W., Hosford, W.F., 1967. The Plastic Deformation of Magnesium. Technical report.
Kitahara, T., Ando, S., Tsushida, M., Kitahara, H., Tonda, H., 2007. Deformation behavior of magnesium single crystals in *c*-axis compression. Key Eng. Mater. 345, 129–132.
Knezevic, M., Levinson, A., Harris, R., Mishra, R.K., Doherty, R.D., Kalidindi, S.R., 2010. Deformation twinning in AZ31: influence on strain hardening and texture evolution. Acta Mater. 58 (19), 6230–6242.
Kucherov, L., Tadmor, E.B., 2007. Twin nucleation mechanisms at a crack tip in an hcp material: molecular simulation. Acta Mater. 55 (6), 2065–2074.
Lavrentev, F.F., Pokhil, Y.A., 1975. Relation of dislocation density in different slip systems to work hardening parameters for magnesium crystals. Mater. Sci. Eng. 18 (2), 261–270.
Li, B., Joshi, S.P., Almagri, O., Ma, Q., Ramesh, K.T., Mukai, T. Rate-dependent hardening due to twinning in an ultrafine-grained Magnesium alloy. Acta Mater., doi:10.1016/j.actamat.2011.12.002, in press.
Li, B., Ma, E., 2009. Zonal dislocations mediating twinning in magnesium. Acta Mater. 57 (6), 1734–1743.
Li, Y., Enoki, M., 2007. Evaluation of the twinning behavior of polycrystalline magnesium at room temperature by acoustic emission. Mater. Trans. JIM 48 (6), 1215–1220.
Lilleodden, E., 2010. Microcompression study of Mg (0001) single crystal. Scr. Mater. 62 (8), 532–535.
Long, T.R., Smith, C.S., 1957. Single-crystal elastic constants of magnesium and magnesium alloys. Acta Metall. 5 (4), 200–207.
Ma, Q., El Kadiri, H., Oppedal, A.L., Baird, J.C., Horstemeyer, M.F., Cherkaoui, M., 2011. Twinning and double twinning upon compression of prismatic textures in an AM30 magnesium alloy. Scr. Mater. 64 (9), 813–816.
Marshall, D.B., McLaren, A.C., 1977. Elastic twinning in experimentally deformed plagioclase feldspars. Phys. Status Solidi A 41 (1), 231–240.
Meyers, M.A., Vöringer, O., Lubarda, V., 2001. The onset of twinning in metals: a constitutive description. Acta Mater. 49 (19), 4025–4039.
Miura, H., Yang, X., Sakai, T., Nogawa, H., Miura, S., Watanabe, Y., Jonas, J.J., 2005. High temperature deformation and extended plasticity in Mg single crystals. Philos. Mag. 85 (30), 3553–3565.
Nave, M.D., Barnett, M.R., 2004. Microstructures and textures of pure magnesium deformed in plane-strain compression. Scr. Mater. 51 (9), 881–885.
Obara, T., Yoshinga, H., Morozumi, S., 1973. $\{11-22\}\langle -1-123\rangle$ Slip system in magnesium. Acta Metall. 21 (7), 845–853.
Park, S.H., Hong, S.G., Lee, C.S., 2010. Activation mode dependent {10−12} twinning characteristics in a polycrystalline magnesium alloy. Scr. Mater. 62 (4), 202–205.
Peirce, D., Asaro, R., Needleman, A., 1982. An analysis of nonuniform and localized deformation in ductile single crystals. Acta Metall. 30 (6), 1087–1119.
Proust, G., Tomé, C.N., Kaschner, G.C., 2007. Modeling texture, twinning and hardening evolution during deformation of hexagonal materials. Acta Mater. 55 (6), 2137–2148.
Randle, V., Engler, O., 2000. Introduction to Texture Analysis—Macrotexture, Micotexture and Orientation Mapping. CRC Press, United Kingdom.
Reed-Hill, R.E., 1960. A study of the {10−11} and {10−13} twinning modes in magnesium. Trans. Metall. Soc. AIME 218, 554–558.
Reed-Hill, R.E., Robertson, W.D., 1958. Pyramidal slip in magnesium. Trans. Metall. Soc. AIME 212, 256–259.
Reed-Hill, R.E., Robertson, W.D., 1957a. Additional modes of deformation twinning in magnesium. Acta Metall. 5 (12), 717–727.
Reed-Hill, R.E., Robertson, W.D., 1957b. The crystallographic characteristics of fracture in magnesium single crystals. Acta Metall. 5 (12), 728–737.
Reed-Hill, R.E., 1960. A study of the {10−11} and{10−13} twinning modes in magnesium. Trans. Am. Inst. Min. Metall. Eng. 218 (3), 554–558.
Remy, L., 1978. Kinetics of f.c.c. deformation twinning and its relationship to stress–strain behaviour. Acta Metall. 26 (3), 443–451.
Roberts, C., 1960. Magnesium and its Alloys. Wiley, New York.

Please cite this article as: Zhang, J., Joshi, S.P., Phenomenological crystal plasticity modeling and detailed micromechanical investigations of pure magnesium. J. Mech. Phys. Solids (2012), doi:10.1016/j.jmps.2012.01.005

Roberts, E., Partridge, P.G., 1966. The accommodation around {1012} ⟨1011⟩ twins in magnesium. Acta Metall. 14 (4), 513–527.
Robson, J.D., Stanford, N., Barnett, M.R., 2011. Effect of precipitate shape on slip and twinning in magnesium alloys. Acta Mater. 59 (5), 1945–1956.
Roters, F., Eisenlohr, P., Hantcherli, L., Tjahjanto, D.D., Bieler, T.R., Raabe, D., 2010. Overview of constitutive laws, kinematics, homogenization and multiscale methods in crystal plasticity finite-element modeling: theory, experiments, applications. Acta Mater. 58 (4), 1152–1211.
Salem, A.A., Kalidindi, S.R., Semiatin, S.L., 2005. Strain hardening due to deformation twinning in α-titanium: constitutive relations and crystal-plasticity modeling. Acta Mater. 53 (12), 3495–3502.
Schmid, E., Boas, W., 1968. Plasticity of Crystals with Special Reference to Metals. Chapman & Hall, London.
Serra, A., Pond, R.C., Bacon, D.J., 1991. Computer simulation of the structure and mobility of twinning disclocations in H.C.P. metals. Acta Metall. Mater. 39 (7), 1469–1480.
Serra, A., Bacon, D.J., 1995. Computer simulation of screw dislocation interactions with twin boundaries in H.C.P. metals. Acta. Metall. Mater. 43 (12), 4465–4481.
Serra, A., Bacon, D.J., Pond, R.C., 1999. Dislocations in interfaces in the h.c.p. metals—I. Defects formed by absorption of crystal dislocations. Acta Mater. 47 (5), 1425–1439.
Slutsky, L., Garland, C., 1957. Elastic constants of magnesium from 4.2 K to 300 K. Phys. Rev. 107 (4), 972–976.
Stanford, N., Barnett, M.R., 2009. Effect of particles on the formation of deformation twins in a magnesium-based alloy. Mater. Sci. Eng. A 516 (1–2), 226–234.
Staroselsky, A., Anand, L., 1998. Inelastic deformation of polycrystalline face centered cubic materials by slip and twinning. J. Mech. Phys. Solids 46 (4), 671–673 675–696.
Staroselsky, A., Anand, L., 2003. A constitutive model for hcp materials deforming by slip and twinning application to magnesium alloy AZ31B. Int. J. Plast. 19 (10), 1843–1864.
Stohr, J., Poirier, J., 1972. Electron microscope study of pyramidal slip {11−22} ⟨11−23⟩ in magnesium. Philos. Mag. 25, 1313–1329.
Tomé, C.N., Lebensohn, R.A., Kocks, U.F., 1991. A model for texture development dominated by deformation twinning: application to zirconium alloys. Acta. Metall. Mater. 39 (11), 2667–2680.
Wang, H., Wu, P.D., Tomé, C.N., Huang, Y., 2010. A finite strain elastic–viscoplastic self-consistent model for polycrystalline materials. J. Mech. Phys. Solids 58 (4), 594–612.
Wang, J., Hirth, J.P., Tomé, C.N., 2009. 10−12 Twinning nucleation mechanisms in hexagonal-close-packed crystals. Acta Mater. 57 (18), 5521–5530.
Wonsiewicz, B.C., 1966. Plasticity of Magnesium Crystals. Ph.D. Thesis. Massachusetts Institute of Technology.
Xu, S., Gharghouri, M.A., Sahoo, M., 2007. Tensile-compressive creep asymmetry of recent die cast magnesium alloys. Adv. Eng. Mater. 9 (9), 807–812.
Yoo, M.H., 1981. Slip, twinning, and fracture in hexagonal close-packed metals. Metall. Mater. Trans. A 12 (3), 409–418.
Yoo, M.H., Wei, C.T., 1967. Slip modes of hexagonal-close-packed metals. J. Appl. Phys. 38 (11), 4317–4322.
Yoshinaga, H., Horiuchi, R., 1963a. Deformation mechanisms in magnesium single crystals compressed in the direction parallel to hexagonal axis. Trans. Jpn. Inst. Met. 4, 1–8.
Yoshinaga, H., Horiuchi, R., 1963b. On the nonbasal slip in magnesium crystals. T Jpn. Inst. Met. 5, 14–21.
Yoshinaga, H., Obara, T., Morozumi, S., 1973. Twinning deformation in magnesium compressed along the *C*-axis. Mater. Sci. Eng. 12 (5–6), 255–264.
Yu, Q., Shan, Z.W., Li, J., Huang, X., Xiao, L., Sun, J., Ma, E., 2010. Strong crystal size effect on deformation twinning. Nature 463 (7279), 335–338.
Zhong, X.L., Wong, W.L.E., Gupta, M., 2007. Enhancing strength and ductility of magnesium by integrating it with aluminum nanoparticles. Acta Mater. 55 (18), 6338–6344.

Please cite this article as: Zhang, J., Joshi, S.P., Phenomenological crystal plasticity modeling and detailed micromechanical investigations of pure magnesium. J. Mech. Phys. Solids (2012), doi:10.1016/j.jmps.2012.01.005